ACS Catalysis

Research Article

pubs.acs.org/acscatalysis

Low-Temperature CO Oxidation Catalyzed by Free Palladium Clusters: Similarities and Differences to Pd Surfaces and Supported Particles

Sandra M. Lang,[†] Irene Fleischer,[†] Thorsten M. Bernhardt,*[,†] Robert N. Barnett,[‡] and Uzi Landman*[,‡]

[†]Institute of Surface Chemistry and Catalysis, University of Ulm, Albert-Einstein-Allee 47, 89069 Ulm, Germany

[‡]School of Physics, Georgia Institute of Technology, Atlanta, Georgia 30332-0430, United States

Supporting Information

ABSTRACT: The catalytic low-temperature oxidation of CO to CO_2 with molecular oxygen is of particular industrial and ecological interest. Gas-phase reaction kinetics measurements in conjunction with first-principles calculations provide comprehensive insight into the mechanisms and energetics of the low-temperature CO combustion reaction catalyzed by small free palladium clusters Pd_x^+ ($x = 2-7$). Similar to the cases of extended palladium single crystals and supported nanoparticles, the catalytic activity of the free palladium clusters was found to be largely determined by the fast adsorption and dissociation of molecular oxygen and the binding strength of carbon monoxide. In particular, Pd_4^+, Pd_5^+, and Pd_6^+ were found to catalyze the oxidation of CO at room temperature, with Pd_6^+ being most active. Detailed mechanistic investigations of the CO oxidation reaction catalyzed by Pd_6^+ reveal a Langmuir–Hinshelwood reaction mechanism, similar to that found earlier for CO oxidation on palladium single crystals, with comparable energetics. The main difference, however, between the cases of small clusters and extended surfaces arises from a considerably reduced bonding of CO to the Pd_6^+ cluster compared to the adsorption strength on the Pd(111) surface, as well as in comparison with the other investigated clusters. This lower CO binding energy prevents CO poisoning at, and below, room temperature, and enables effective low-temperature CO oxidation. Consequently, this study shows that free clusters can serve as model systems for mechanistic studies of catalytic reactions at the molecular level, in addition to opening new ways for the rational design of effective low-temperature CO oxidation catalysts through tunability of the reaction parameters by changing the number of constituent atoms.

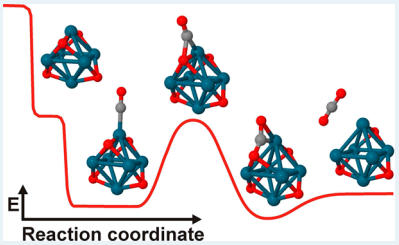

KEYWORDS: *gas-phase reaction, catalysis, CO oxidation, palladium clusters, density functional theory*

1. INTRODUCTION

Palladium is one of the most widely employed materials for heterogeneous oxidation catalysts. The particular industrial and scientific interest in palladium originates from its ability to catalyze the CO combustion reaction and its resulting technological and environmental relevance for the automotive catalytic converter.[1] However, the main problem of today's three-way catalytic converters is the rather high operation temperature of at least 570 K, inhibiting the conversion of pollutants in the start-up period.[2] For the targeted development and optimization of new low-temperature catalysts, a molecular level understanding of the energetics and kinetics of the elementary processes involved in the overall catalytic CO oxidation reaction is of essential importance.

Industrial heterogeneous catalysts usually represent extremely complex systems composed of small metal particles dispersed on porous materials, which inhibits the detailed investigation of principal parameters and elementary reaction mechanisms. Consequently, to gain basic insight into the chemical properties and catalytic activity of palladium, numerous studies on simplified model systems like extended Pd single crystal surfaces, supported nanoparticles, small supported clusters, and also small gas phase clusters have been performed during the past several decades. Although these models represent systems of varying complexity, and although the experiments were performed over a large range of experimental conditions, these methods turned out to be highly complementary and already revealed a number of pertinent details about the catalytic CO combustion reaction. To put our paper in context and to provide a framework for the discussion of our gas-phase cluster experiments and first-principles theoretical simulations, we first overview certain pertinent findings from earlier studies.

1.A. Pd Single Crystals. Ordered extended metal surfaces are structurally well-characterized, and their properties have been well-studied for the past several decades, thus making them well-suited as a model system for the investigation of heterogeneous catalysis. Indeed, more than three decades ago, Ertl and co-workers showed that the oxidation reaction of CO proceeds on palladium single crystals via a complex reaction mechanism of the Langmuir–Hinshelwood (LH) type. These authors have identified two key factors which determine the

Received: June 10, 2014
Revised: January 22, 2015
Published: March 11, 2015

DOI: 10.1021/cs5016222
ACS Catal. 2015, 5, 2275–2289

efficiency of this reaction:[3] (1) the dissociative chemisorption of oxygen on the catalyst surface and (2) the adsorption strength of carbon monoxide.[3b] Once CO and dissociated oxygen are simultaneously formed on the palladium surface, the formation and desorption of CO_2 was observed to be fast,[3a,4] and the LH activation barriers for the total CO combustion reaction were experimentally determined by two different groups to amount to 105 ± 8 kJ mol^{-1}[3b] and 118 ± 1 kJ mol^{-1},[4] respectively, at low CO coverages (T > 500 K) and to 59 ± 8 kJ mol^{-1}[3b] at moderate CO coverages (T < 500 K).

On Pd single crystals, O_2 adsorption and dissociation proceed essentially without an activation barrier[3b] and were observed to occur even at temperatures as low as 200 K.[5] In contrast, CO adsorbs nondissociatively with binding energies ranging between 129 kJ mol^{-1} and 185 kJ mol^{-1} at low CO coverages, depending on the CO coverage and the applied analytical method.[4,6]

These rather high CO adsorption energies cause a fast covering (saturation) of the catalyst surface with CO, which inhibits O_2 coadsorption at low temperatures and leads to catalyst poisoning. As a result, a reaction temperature of at least around 450 K is required to enable CO_2 formation.[1,3b] Consequently, the rate-limiting step of the reaction is believed to be the desorption of CO molecules to liberate O_2 adsorption sites, which in turn determines the rate of oxygen adsorption.[4] However, due to a rather complicated mutual interaction of the reactants as a function of the surface coverage and the temperature, it was not possible to formulate simple kinetic schemes for the reaction, valid over the entire range of accessible temperature and pressure conditions.[3b,7]

The formation of oxides on metal surfaces has received much attention over the years, with a surge in surface science research efforts in this area taking place for a little over a decade now. In addition to the fundamental importance of understanding oxidation processes that are often associated with corrosion, metal surface oxidation, for selected conditions, can lead to the growth of oxide layers, which can be employed as protective coating against corrosion, as insulating layers in microelectronic devices, and, most pertinent for this paper, as catalytic substrates even where the catalytic behavior has been attributed in the past to the bare metal surface.[8] For late transition metals and noble metals (e.g., Pd and Ag), it has been demonstrated that oxidation proceeds through formation of ultrathin (down to monolayer thickness) thermodynamically stable oxide layers that may be of high structural complexity[9] and may exhibit structural properties unrelated to the metal structure or to the bulk oxides;[9] see, in particular, the complex structure of the "surface oxide" formed on Pd(111) from the Pd_5O_4 adsorbate unit cell, as found from combined scanning tunneling microscopy, surface X-ray diffraction, high-resolution core level spectroscopy, and density functional calculations.[9b] It has been concluded[9b] that from consideration of both the structural and energetic aspects of the system under study, the ultrathin surface oxide (of subnanometer thickness, with the core level energies calculated for the Pd layer directly below the surface oxide layer being almost exactly the same as for bulk Pd) is an intermediate phase between an oxygen overlayer (that is surface-adsorbed oxygen) and a bulk oxide, and as such, it could have interesting consequences for heterogeneous catalysis. It is pertinent to remark[9b] that the above findings contrast earlier views where it was assumed that oxygen on metal surfaces forms either overlayers, sometimes causing simple rearrangements of the metal atoms such as vacancies[10] or additional metal atoms[11] at lattice sites, or causes the formation of oxides, which were believed to be identical or closely related to the corresponding bulk oxides; a larger variety of structures have been observed in oxides of one metal grown on a different metal (see, e.g., ref 12 and references therein).

Although the formation of different oxygen species is assumed to strongly influence the catalytic activity, the detailed role of different oxygen species remains largely elusive. Systematic studies[8b] identified dissociatively adsorbed surface oxygen, O(ad), as the most reactive species on both Pd(100) and Pd(111) surfaces, followed by the reactivity of the aforementioned Pd_5O_4 surface oxide[9b] on Pd(111), which reacted with CO at a higher temperature (330 K compared to 223 K for CO oxidation on O(ad)/Pd(111), with the catalytic activities of the two systems becoming comparable at 400 K). On the other hand, continuous (substoichiometric) PdO_x layers were found to be much less reactive toward CO, and PdO did not react with CO below 493 K even around 10 mbar (probably due to the lack of adsorption sites for CO on bulk PdO as compared to the Pd_5O_4 surface oxide).[8b]

1.B. Supported Pd Nanoparticles. Despite the important fundamental knowledge gained in experimental studies on Pd single crystals, these model systems cannot account for all characteristics of technical catalysts. In particular, the finite size of the catalytically active metal particles as well as the interaction between the metal particles and the support material requires more complex model systems which can be found (e.g., in palladium nanoparticles supported on well-defined single crystalline (thin film) oxide surfaces).[13] One particularly important issue in these systems is the determination of particle size effects which, however, turned out to be difficult, and thus, it remained for a rather long time unclear to what an extent size effects control the kinetics and energetics of the CO combustion reaction (see ref 13a and references therein).

Palladium nanoparticles were found to form a variety of oxygen species, like interfacial, surface, subsurface, and bulk oxygen or PdO-like oxide shells, depending on the applied reaction conditions and also on particle size.[14] Similar to extended Pd single-crystal surfaces, dissociative O_2 adsorption on Pd nanoparticles was observed at temperatures as low as 200 K.[14a] Hence, O_2 adsorption and dissociation occurs already well below room temperature also on Pd particles and should not be the rate-determining reaction step for low-temperature CO oxidation. However, only oxygen atoms chemisorbed on the metallic Pd nanoparticles have so far been identified to be directly involved in the CO oxidation reaction, whereas oxide layers formed at the metal/support interface of, for example, Fe_3O_4-supported nanoparticles, were found to only serve as an oxygen reservoir.[14d]

With respect to the binding energy of CO on palladium nanoparticles, temperature-programmed desorption and modulated molecular beam studies revealed no clear particle-size-dependent trend. For example, Henry and co-workers observed an increase in the CO binding energy for particles smaller than 5 nm supported on MgO(100) (increase of more than 33.5 kJ mol^{-1} for a 2 nm particle compared to a Pd single crystal).[6f,15] In contrast, Stará et al. detected a decrease of about 11 kJ mol^{-1} for a 2.5 nm particle on Al_2O_3 compared to Pd(111).[16] Direct calorimetric measurements of the CO heat of adsorption demonstrated a reduction by up to 42 kJ mol^{-1} for a 1.8 nm particle on a well-ordered Fe_3O_4/Pt(111) film as compared to Pd(111).[17] Furthermore, CO was found to dissociate on

DOI: 10.1021/cs5016222
ACS Catal. 2015, 5, 2275−2289

palladium nanoparticles (see ref 13a and references therein). Most recently, Henry and co-workers reported a study of CO adsorption on regular, almost monodisperse arrays of Pd particles on nanostructured alumina ultrathin films. This investigation revealed a highly discontinuous evolution of the CO adsorption energy with particle size in the range between 1 and 2 nm of the particles' diameters, with values as low as 30 kJ mol^{-1}.[18]

Particle size effects appear to be currently rather ambiguous not only with respect to the interaction of O_2 and CO with palladium nanoparticles but also related to the complete catalytic CO oxidation reaction. In agreement with studies on Pd single crystals, the reaction was found to proceed via a Langmuir−Hinshelwood mechanism.[14a,d,19] For particles with an average 5.5 nm diameter supported on Al_2O_3 the Langmuir−Hinshelwood activation energy was experimentally determined to be 57 ± 6 kJ mol^{-1} at high CO and low oxygen coverage and 62 ± 8 kJ mol^{-1} at low CO and high oxygen coverage,[14a] which is in excellent agreement with the activation barrier determined for Pd(111) in the lower-temperature regime (<500 K), that is, 59 ± 8 kJ mol^{-1}.[3b] In contrast, in a different study, a strongly decreasing activation energy with decreasing particle size was observed, that is, 45−64 kJ mol^{-1} for Pd(111), 32−45 kJ mol^{-1} for 27 nm Pd/Al_2O_3, and 19−20 kJ mol^{-1} for 2.5 nm Pd/Al_2O_3. This indicates an increased catalytic activity for smaller particles.[19]

In summary, the overall features of the catalytic CO combustion reaction mediated by supported Pd nanoparticles are similar to those observed on extended Pd single crystals: (1) The reaction proceeds via a Langmuir−Hinshelwood reaction mechanism; (2) Molecular oxygen adsorbs dissociatively on Pd nanoparticles even at temperatures below 300 K; (3) CO adsorption energies are comparable to those of Pd surfaces over a wide particle size range resulting in required reaction temperatures well above room temperature to avoid catalyst poisoning. Only small particles with diameters of a few nanometers seem to exhibit size effects.

As an explanation for these surprising observations in the very small size range, formation of subsurface oxygen as the reactive oxidant species on small particles has been inferred.[13a] Additionally, it is reasonable to expect that different CO adsorption sites on defects like corners, edges, and kinks, whose relative abundance increases with decreasing particle size, may contribute to the changed catalytic activity. Furthermore, for supported small particles,[13a] precursor state effects (e.g., the capture of molecules first physisorbed on the oxide support) may affect considerably the energetics and kinetics of the overall reaction.

1.C. Small Supported Clusters. As detailed above, experimental studies on supported nanoparticles indicated size effects in the catalytic CO combustion reaction for very small particles of only a few nanometers in size. Even more pronounced size effects can be expected for clusters in the so-called nonscalable size regime[20] (up to about 100 atoms per cluster) where the particle properties change nonmonotonically with cluster size. However, studies of such model systems are more scarce.

Magnesia-supported palladium atoms and clusters, Pd_x/MgO/Mo(100), comprising up to 30 atoms were observed to catalyze the CO oxidation reaction already at 300 K and below.[21] This finding was interpreted by a reduced CO binding energy on these small clusters compared to single crystals resulting in the availability of unoccupied O_2 adsorption sites and thus enabling CO oxidation already at lower temperatures. Most interestingly, preadsorbed CO was even found to promote oxygen adsorption and dissociation in the temperature range of 300−420 K instead of blocking possible oxygen adsorption sites as on single crystals.[21b] A cooperative Langmuir−Hinshelwood mechanism was proposed to describe the observed reaction behavior, and these results revealed for the first time details of the coadsorption effects between O_2 and CO.[21b] Furthermore, comprehensive combined experimental and theoretical studies[21d] indicated a competition between a Mars−van Krevelen[22] and a Langmuir−Hinshelwood type reaction mechanism for the CO oxidation catalyzed by Pd_{30}/MgO depending on the reaction temperature; a similar result was found[21c] also for Pd_{13}/MgO. Concerning the oxidation state of the clusters, the low-symmetry palladium oxide $Pd_{13}O_6$/MgO was found[21c] to exhibit smaller activation barriers for CO oxidation compared to the highly symmetric $Pd_{13}O_4$/MgO.[21c]

In a different experiment, strong size effects in the oxidation of CO mediated by $Pd_x/TiO_2(110)$ (x = 1−25) have been found to correlate with the oxygen activation efficiency, which in turn was attributed to variations in the cluster electronic structure.[23] It was suggested that the formation of reactive oxygen is an activated process for all cluster sizes and that this represents the limiting factor that largely determines the size-dependent activity. However, XPS studies have shown that small clusters Pd_x (x = 1, 7, 10, 13) supported on alumina are efficiently oxidized by exposure to O_2 already at 100 K with no or little activation barrier, whereas no oxidation was found for Pd_4.[24] Subsequent theoretical studies attributed this behavior to an anomalously small charge donation from Pd_4 to the adsorbed O_2 due to an enhanced stability of Pd_4.[25]

Density functional theory studies on small magnesia-supported palladium clusters revealed an unexpected low dissociation barrier (48 kJ mol^{-1}) for O_2 on Pd_9/MgO, implying that the O_2 dissociation reaction should be observable well below room temperature on this cluster.[26] However, a rather strong adsorption of CO on Pd_9/MgO was found to inhibit subsequent O_2 dissociation resulting in the poisoning of the catalyst. Hence, these results indicate that small Pd clusters will catalyze CO oxidation best under O_2-rich conditions where preformation of crystalline nano-oxide clusters Pd_xO_y is possible. Under these reaction conditions CO_2 formation and adsorption (release) is predicted to involve activation barriers of 60−100 kJ mol^{-1}.[26]

Although the number of studies on small supported clusters is rather limited, there are clear indications for the appearance of nontrivial size effects. In particular, cooperative effects on such small particles may considerably reduce the temperature needed to avoid catalyst poisoning and enable effective CO oxidation. Thus, more detailed studies on cluster-size-specific oxygen activation, CO adsorption, as well as CO_2 formation and desorption processes are desirable.

1.D. Free Clusters. Small clusters in the gas phase may represent model systems for detailed studies on a (rigorous) molecular level.[27] Despite the fact that free clusters cannot account for a number of complex processes occurring in catalytic processes on solid surfaces (particularly involving supported catalytic particles), they can be employed to model the catalytically active centers,[28] that is, the locations where the actual chemical transformations involved in the catalytic reactions take place. Such active sites are usually characterized by a spatial extension on the subnanometer scale and may

DOI: 10.1021/cs5016222
ACS Catal. 2015, 5, 2275−2289

involve defect sites, undercoordinated atoms, or unsaturated bonds, which may be appropriately modeled with the use of small clusters.[29] Hence, the gas phase study of free palladium clusters provides an attractive complementary approach to the other model systems discussed above.

Both anionic[30] and neutral[31] palladium clusters have been found to readily react with molecular oxygen without significant cluster size dependence. Insights into the O_2 binding to the Pd atom has been gained by ultraviolet photoelectron spectroscopy of PdO_2^-, which revealed the dissociation of the oxygen molecule resulting in a linear O−Pd−O geometry in agreement with previous studies.[32] However, the structure of the larger complexes $Pd_xO_2^-$ (x = 2−7) could not be clearly assigned.[30b] Theoretical studies have mainly been performed on selected neutral clusters so far.[33] Detailed investigations of Pd_x (x = 2−4) employing spin density functional theory demonstrated the dissociative adsorption of a first oxygen molecule leading to oxygen atoms sitting on Pd bridge sites.[33a] In agreement with this observation, $Pd_4O_2^{\mp}$ complexes containing activated or dissociated oxygen have been theoretically found to be energetically more favorable than complexes containing molecular oxygen.[33d]

With respect to cationic palladium clusters, energetic collisions of Pd^+ ions with molecular oxygen have been investigated previously.[34] However, only recently, have the details of the cluster-size- and temperature-dependent bonding and activation of molecular oxygen by palladium cluster cations Pd_x^+ (x = 2−7) been reported by the present authors.[35] The results reveal the preferred formation of tetroxide product complexes, $Pd_xO_4^+$ for all investigated cluster sizes, although a strong cluster-size-dependent reactivity toward a first O_2 molecule has been detected. Concomitant theoretical simulations indicated that these palladium tetroxide complexes contain dissociatively chemisorbed oxygen over a large part of the investigated temperature range (100−300 K), whereas additional molecularly adsorbed O_2 was only found at cryogenic temperatures.[35a,36]

In contrast to the reaction with O_2, small anionic[37] and neutral[38] palladium clusters show a more pronounced cluster size specific behavior in the reaction with CO. For cationic Pd_x^+, an enhanced reactivity toward CO with increasing cluster size has recently been observed over a wide temperature range between 100 and 300 K.[39] Most interestingly, the binding energies of a first CO molecule to palladium clusters of all charge states strongly vary with the addition of each Pd atom.[40] Finally, infrared spectroscopic studies of $Pd_x(CO)^{\pm}$ (x = 3−12) revealed the molecular adsorption of a first CO molecule on top, bridge, and hollow sites with varying probabilities.[37c]

Although a considerable number of experimental and theoretical contributions investigate the reaction of free (gas phase) palladium clusters with O_2 or CO separately, there are hardly any studies of such clusters addressing the catalytic CO combustion reaction. Only recently, reactivity studies in an octopole ion trap from this laboratory have revealed the fast formation and desorption of CO_2 after the exposure of preoxidized palladium clusters Pd_xO^+ (x = 3−5) and $Pd_xO_2^+$ (x = 4−6) to CO.[39] In contrast, CO oxidation was less pronounced in the case of Pd_2O^+, Pd_6O^+, and Pd_7O^+, indicating enhanced activation barriers involved in the CO oxidation and/or CO_2 desorption process on these particular cluster monoxides.[39]

Using a different approach, which employed guided-ion-beam mass spectrometry in conjunction with density functional theory calculations, the importance of oxygen radical centers for the CO oxidation capabilities of preoxidized PdO_2^+ and PdO_3^+ has been investigated. These studies gave experimental evidence for both direct and cooperative CO oxidation mechanisms.[41] Finally, the charge-state-dependent interaction of $Pd_4O_y^{\pm}$ (y = 1, 2) with CO was theoretically simulated, predicting an enhanced activity of the cationic and neutral cluster compared to the anionic one.[33d]

So far, investigations of the CO combustion reaction utilizing free Pd clusters focused mainly on the formation and desorption of CO_2 on preoxidized clusters. Similarly, most studies on single-crystal surfaces as well as on supported nanoparticles and clusters, utilized pulsed methods, where palladium oxide is prepared prior to the reaction with CO. In contrast, in a recent contribution, we reported for the first time on a joined experimental gas phase and first-principles DFT study of the room temperature CO oxidation reaction catalyzed by Pd_6^+, where a full thermal catalytic reaction cycle has been revealed.[35a] These experiments were performed with mass-selected Pd_6^+ clusters that were stored in a temperature controlled radio frequency (rf) octopole ion trap where they reacted under multicollision conditions with O_2 and CO (see also Experimental and Computational Methods).

In the work presented here, we have extended the previous room-temperature kinetic investigation and present a full account of the experimental temperature and pressure dependencies. A more comprehensive insight into mechanistic details and the energetics of the catalytic CO oxidation reaction is gained by theoretical simulations, which allow a direct comparison of the energetics of the gas phase reaction with previous studies that were carried out on extended Pd surfaces and nanoparticles. Furthermore, the investigations have been expanded to include other cluster sizes Pd_x^+ (x = 2−7) as well as the palladium mono-oxides Pd_xO^+, in order to gain detailed insight into the role of oxygen adsorption and dissociation as well as the CO binding strength in the complex CO oxidation reaction. In particular, similarities and differences to extended Pd single crystals and supported nanoparticles will be discussed.

2. EXPERIMENTAL AND COMPUTATIONAL METHODS

2.A. Experimental Method. *Experimental Setup.* The gas-phase reactions of small palladium clusters have been studied in an rf octopole ion trap embedded into a low-energy ion beam assembly of quadrupole ion guides and mass spectrometers. The general experimental layout has been described in detail elsewhere[42] and will only be outlined briefly here (more experimental details can also be found in the Supporting Information).

Palladium clusters Pd_x^+ and their oxides Pd_xO^+ are generated by simultaneous sputtering of four preoxidized palladium targets with high-energy Xe ion beams, which are produced in a CORDIS (cold reflex discharge ion source).[43] The formed cluster ion beam is steered into a first helium-filled quadrupole ion guide to collimate and thermalize the hot clusters. Subsequently, cluster ions of the desired size are selected from the beam by means of a mass-selecting quadrupole filter and are transferred via a second quadrupole ion guide into the home-built octopole ion trap. The ion trap is prefilled with about 1 Pa of helium buffer gas and a mixture of O_2 and CO at variable partial pressure ratios (reactant partial pressure typically 1−20% of the total pressure). The ion trap is attached to a closed cycle helium cryostat, which, in combination with a resistive heater, allows for temperature adjustment in the range

DOI: 10.1021/cs5016222
ACS Catal. 2015, 5, 2275−2289

between 20 and 300 K. Thermal equilibration of the clusters is achieved within a few milliseconds under our experimental conditions,[42] whereas the clusters are stored in the ion trap for a considerably longer time, typically between 0.1 s and several seconds. The CO oxidation reaction occurs under thermal conditions in the ion trap experiment and thus proceeds on the electronic ground state potential energy surface.

After reaction of the clusters in the ion trap for a chosen time (reaction time t_R) all ions, intermediates, and final products are extracted, and the ion distribution is analyzed in a second quadrupole mass filter. Kinetic data are obtained by recording the intensity of all ion signals as a function of the reaction time. The normalized kinetic traces are then evaluated by fitting the integrated rate equations of potential reaction mechanisms to the experimental data utilizing the software package "Detmech".[44] This leads to the determination of the simplest reaction mechanism that best fits the experimental data.

Data Evaluation. To analyze the differences in the catalytic activity of the investigated Pd_x^+ clusters, it is necessary to briefly introduce the reaction models underlying the experimentally determined reactions.

The total pressure inside the ion trap is about 1 Pa, which means that the experiments are performed in the kinetic low-pressure regime. Therefore, the details of each association reaction between a palladium cluster Pd_x^+ and a neutral molecule L (L = O_2, CO)

$$Pd_x^+ + L \rightarrow Pd_xL^+ \qquad k_1 \tag{1}$$

can be described by the Lindemann energy transfer model for association reactions (k_1 is the corresponding rate constant),[45] which is represented by the following elementary reaction steps

$$Pd_x^+ + L \rightleftarrows (Pd_xL^+)^* \qquad k_a, k_d \tag{2a}$$

$$(Pd_xL^+)^* + He \rightarrow Pd_xL^+ + He^* \qquad k_s \tag{2b}$$

According to this model, Pd_x^+ reacts with the neutral molecule L (rate constant k_a) under formation of an energized complex $(Pd_xL^+)^*$. This complex can either decompose unimolecularly back to the reactants (k_d) or can be stabilized by a collision with helium buffer gas (k_s). Consequently, the measured overall reaction rate k_1 depends on both, the helium and the reactant concentration [He] and [L], respectively. Furthermore, the cluster ion concentration in the ion trap is orders of magnitude smaller than [He] and [L], and additionally, a steady flow of the reactants and the buffer gas is ensured, which permits the postulation of pseudo-first-order kinetics. Under the applied low pressure multicollision conditions, the decomposition rate constant k_d is typically orders of magnitude larger than the stabilization k_s[He] (k_d is usually on the order of 10^7 to 10^{11} s^{-1}, whereas k_s amounts to about $5\cdot10^{-10}$ cm^3 s^{-1}, and hence $k_s\cdot$[He] = $10^5 s^{-1}$).[46] Thus, the stabilization of the energized complex $(Pd_xL^+)^*$ is the rate-determining reaction step, and the pseudo-first-order rate constant in the low pressure limit is given by

$$k_1 = k^{(3)}[L][He] = k_a k_s / k_d [L][He] \tag{3}$$

The rate constants k_a and k_s are well represented by ion−molecule collision rate constants, as specified by Langevin theory,[45a,47] and are largely temperature independent. Thus, any experimentally observed temperature dependence must be contained in the unimolecular decomposition rate constant k_d. The activation barrier of this decomposition reaction results in an increase of the reaction rate with decreasing temperature for simple association reactions because the lifetime of the energized complex $(Pd_xL^+)^*$ increases with decreasing temperature, and stabilizing collisions become much more effective at lower temperatures. As a result, the number of adsorbed molecules on the cluster typically increases with decreasing temperature because more weakly bound complexes can also be stabilized at lower temperatures.[46]

In contrast, desorption of the molecule L from a formed and stabilized complex Pd_xL^+

$$Pd_xL^+ \rightarrow Pd_x^+ + L \qquad k_{-1} \tag{4}$$

represents an activated process and can be described by the Lindemann mechanism[45a]

$$Pd_xL^+ + He^* \rightleftarrows (Pd_xL^+)^* + He \qquad k_e, k_s \tag{5a}$$

$$(Pd_xL^+)^* \rightarrow Pd_x^+ + L \qquad k_d \tag{5b}$$

In this model, the cluster complex Pd_xL^+ collides with an energy-rich He* atom and becomes energized $(Pd_xL^+)^*$ (rate constant k_e). Such an energized molecule can then either be de-energized (stabilized) by collision with a further He atom (k_s) or can decompose unimolecularly into Pd_x^+ and L (k_d). However, the desorption of L (decomposition of Pd_xL^+) is only possible if the helium atom He* transfers enough energy to overcome the energy barrier for dissociation. In the low-pressure regime, the rate constant for energization thus represents the rate-limiting reaction step and the overall desorption rate constant k_{-1}

$$k_{-1} = k_e[He] \tag{6}$$

only depends on the helium pressure and the rate constant for energization. Because the number of He* containing enough energy for energization is determined by the Boltzmann distribution and thus the reaction temperature, k_{-1} typically decreases with decreasing temperature.

2.B. Theoretical Methods. The theoretical explorations of the atomic arrangements and electronic structures of the Pd_6^+ cluster and its complexes were performed with the use of first-principles density functional theory (DFT) calculations. In particular, we employed the Born−Oppenheimer (BO)−spin density functional (SDF)−molecular dynamics (MD) method, BO−SDF−MD[48] with norm-conserving soft (scalar relativistic for Pd) pseudopotentials[49] and the generalized gradient approximation (GGA)[50] for electronic exchange and correlations. In these calculations, we have used a plane-wave basis with a kinetic energy cutoff E_c = 110 Ry, which yields convergence. This corresponds to a real-space grid spacing of 0.3 a_0; the real-space grid spacing for the density was 0.1 a_0 corresponding to E_c = 987 Ry. In the construction of the Pd pseudopotentials, the valence electrons, $4s^2$, $4p^6$, and $4d^{10}$, were characterized by core radii r_c = 0.85 a_0, 0.90 a_0, and 1.15 a_0, respectively, with the s orbital treated as local; a_0 is the Bohr radius. The BO−SDF−MD method is particularly suitable for investigations of charged systems because it does not employ a supercell (i.e., no periodic replication of the ionic system is used). In all the calculations, the dependence on spin multiplicity has been checked, and the results that we report correspond to the spin multiplicities with the lowest energies; for early prediction of the magnetic properties of palladium clusters, see ref 51. Structural optimizations were performed using a conjugate-gradient-like method.

DOI: 10.1021/cs5016222
ACS Catal. 2015, 5, 2275−2289

In the first-principles calculations of the reaction profiles (pathways), a reaction coordinate was judiciously chosen; typically, the reaction coordinate consists of the distance between two atoms of the reactant molecules (for example an O atom of an adsorbed oxygen molecule and the C atom of a reacting CO molecule). For each value of the reaction coordinate, the total energy of the system was optimized through unconstrained relaxation of all of the other degrees of freedom of the system (reactants, other adsorbents, and Pd cluster atoms). The reaction profiles (reaction paths) were obtained via repeating such calculations for various values of the chosen reaction coordinate. These calculations yield results that are the same as, or close to, those obtained by other methods (e.g., the nudged elastic band and variants thereof); see the discussion on pp 89 and 90 in ref 20f.

3. RESULTS AND DISCUSSION

3.A. Rate Constants for O_2 and CO Adsorption and Desorption. Among all the investigated clusters, Pd_2^+, Pd_3^+, and the oxides Pd_2O^+ and Pd_3O^+ rapidly decompose via loss of neutral Pd atoms upon reaction with CO under the applied experimental conditions.[39] Furthermore, Pd_7^+ and Pd_7O^+ were found to fragment after the reaction with O_2 as well, exclusively yielding the stable six-atomic palladium-oxide $Pd_6O_4^+$.[35a,36] Similar fragmentation behavior of these clusters was also observed in the presence of an O_2/CO mixture. Thus, Pd_2^+, Pd_3^+, and Pd_7^+ (as well as the corresponding oxides) are not suitable model systems for a detailed investigation of the CO oxidation reaction and will not be discussed further here; instead, we will focus exclusively on the palladium clusters Pd_4^+, Pd_5^+, and Pd_6^+ (as well as on the corresponding mono-oxides).

Figure 1a displays the experimentally obtained termolecular rate constants $k^{(3)}$ (cf. eqs 1−3, Experimental and Computational Methods) for the adsorption of a first O_2 molecule (black squares) onto Pd_x^+ (x = 4−6).[35b,36] These data show the increasing reactivity of these Pd clusters toward O_2 with increasing clusters size (see also Table 1). In contrast, the rate constant for the adsorption of a first CO molecule is similar for Pd_4^+ and Pd_6^+, whereas Pd_5^+ shows enhanced reactivity (Figure 1a, red circles, and Table 1). In this latter case, due to the fast reaction of Pd_x^+ with CO even at low CO partial pressure,[39] the experimental determination of reliable rate constants was only possible for Pd_4^+ (green triangle in Figure 1a). Therefore, the rate constants describing the CO adsorption reaction have been deduced from theoretical binding energies[40h] by employing RRKM theory[52] and the Lindemann energy transfer model for association reactions[45a] (red circles in Figure 1a, cf. eq 2 in Experimental and Computational Methods). For Pd_4^+ the thus obtained value amounts to 61 × 10^{-27} $cm^6\ s^{-1}$, which is in excellent agreement with the experimental value listed in Table 1.

The desorption of O_2 and CO, respectively, from the once formed and stabilized complexes $Pd_xO_2^+$ and Pd_xCO^+ is an activated process that can be described by a Lindemann-type reaction schema,[45a] as detailed in eq 5 (Experimental and Computational Methods). Under the applied low-pressure conditions (total pressure of about 1 Pa), the overall reaction rate constant k_{-1} for the desorption of the ligands (reaction eq 4 in Experimental and Computational Methods) can be considered to be determined by the energization of $Pd_xO_2^+$ and Pd_xCO^+ via collision with an energy-rich He* atom (eqs 5a, 5b, and 6, Experimental and Computational Methods). The experimentally obtained energization rate constants k_e for

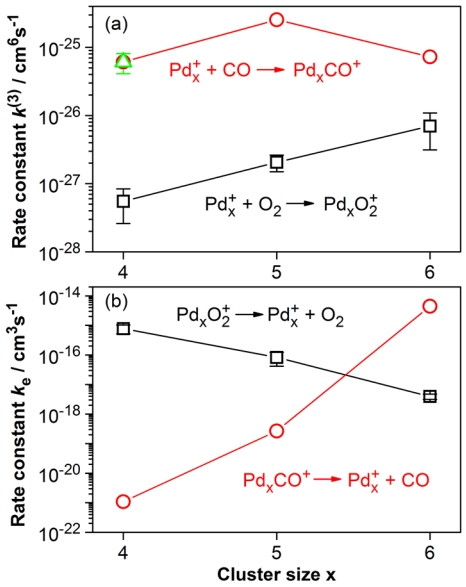

Figure 1. (a) Experimentally obtained termolecular rate constant $k^{(3)}$ for the adsorption of a first O_2 molecule (black squares) onto Pd_x^+ (x = 4−6) and of a first CO molecule onto Pd_4^+ (green triangle). The rate constants $k^{(3)}$ for the reaction $Pd_x^+ + CO \rightarrow Pd_xCO^+$ (red circles) have been deduced from theoretical Pd_x^+-CO binding energies[40h] by employing RRKM theory[52] and the Lindemann energy transfer model for association reactions (see Experimental and Computational Methods).[45a] (b) Energization rate constants, k_e (cf. eqs 4−6), for the desorption of the ligands from the stabilized complexes $Pd_xO_2^+$ (black squares, experimental values) and Pd_xCO^+ (red circles, estimated values obtained by applying the Hinshelwood−Lindemann theory[45a]). Lines are only drawn as a guide to the eye.

Table 1. Termolecular Rate Constants $k^{(3)}$ for the Adsorption of a First O_2 and CO Molecule, Respectively, On Different Palladium Clusters Pd_x^+ as well as Energization Rate Constants k_e for the Ligand Desorption from the Complexes $Pd_xO_2^+$ and Pd_xCO^+

Pd_x^+	$k^{(3)}(O_2)$ [$10^{-27}cm^6s^{-1}$]^a	$k^{(3)}(CO)$ [$10^{-27}cm^6s^{-1}$]	$k_e(Pd_xO_2^+)$ [$10^{-17}cm^3s^{-1}$]^a	$k_e(Pd_xCO^+)$ [$10^{-17}cm^3s^{-1}$]^b
Pd_4^+	0.55 ± 0.29	61 ± 20^a	78 ± 26	0.00011
Pd_5^+	2.1 ± 0.6	250^b	8.2 ± 4.1	0.027
Pd_6^+	7.0 ± 3.9	73^b	0.39 ± 0.08	443

^{a}Experimentally obtained values. ^{b}Estimated values; for details, see text.

$Pd_xO_2^+$ are displayed in Figure 1b as black squares (cf. Table 1), illustrating a decreasing probability for O_2 desorption with increasing cluster size. In contrast, the energization rate constants k_e for Pd_xCO^+ (red circles in Figure 1b), which have been estimated by employing the Hinshelwood−Lindemann theory,[45a] demonstrate a strongly increasing CO desorption probability with increasing cluster size.

Comparing the cluster-size dependence of the rate constants for the oxygen adsorption with the corresponding rate constants for oxygen ligand desorption in Figure 1 and Table 1 reveals that O_2 most strongly reacts with Pd_6^+, and accordingly, the desorption of O_2 from $Pd_6O_2^+$ is the slowest among all investigated clusters. The comparably large desorption rate constant of O_2 from Pd_4^+ was explained by theoretical simulations to be due to the molecular adsorption and subsequent activated dissociation of O_2 on this particular cluster.[36] In contrast, a reverse cluster-size dependence of k_e is

DOI: 10.1021/cs5016222
ACS Catal. 2015, 5, 2275−2289

observed for Pd_xCO^+. The rather high CO binding energy on Pd_4^+ (132 kJ mol^{-1}[40h]) and Pd_5^+ (127 kJ mol^{-1}[40h]) results in very small desorption rate constants for these cluster sizes, whereas the reduced CO binding energy on Pd_6^+ (103 kJ mol^{-1}[40h]) leads to an increase of k_e by several orders of magnitude.

Interestingly, the final products of all three clusters Pd_{4-6}^+ after reaction with O_2 under thermal equilibrium conditions are exclusively the tetra-oxide complexes $Pd_xO_4^+$.[35a,36] Only at cryogenic temperatures are more weakly bound oxygen molecules adsorbed. In contrast, the reactions with carbon monoxide lead to instant multiple CO adsorption yielding the carbonyl complexes $Pd_4(CO)_{8-10}^+$, $Pd_5(CO)_{9-11}^+$, and $Pd_6(CO)_{9-13}^+$ with the maximum number of adsorbed CO, depending on the reaction temperature.[39]

In the following sections, we will present experimental and theoretical results obtained for the catalytic CO oxidation mediated by the model systems Pd_4^+, Pd_5^+, and Pd_6^+ in order to gain insight into the importance of O_2 adsorption and dissociation on the cluster, as well as of the CO adsorption strength for the low-temperature CO combustion. These data will be interpreted on the basis of the above presented rate constants for ligand adsorption and desorption, and the results will be compared with fundamental findings on extended Pd surfaces, supported Pd nanoparticles, and clusters.

3.B. CO Oxidation Mediated by Pd_4^+. From Figure 1a and Table 1 it is apparent that for all three clusters, Pd_4^+, Pd_5^+, and Pd_6^+, the CO adsorption rate constant exceeds the O_2 adsorption rate constant by at least one order of magnitude. Therefore, in the experiments described in the following, in which the catalytic activity of these clusters is investigated by introducing a mixture of O_2 and CO into the ion trap, an excess of oxygen is always provided to partly compensate for the reactivity differences.

Figure 2 displays the ion mass distribution (Figure 2a) and the corresponding kinetic data (Figure 2b) for the reaction between Pd_4^+ and an 11:1 mixture of O_2 and CO. At these pressure conditions, Pd_4^+ reacts to form the products Pd_4CO^+, $Pd_4O(CO)_5^+$, $Pd_4O(CO)_6^+$, and $Pd_4O_2(CO)_6^+$, with $Pd_4O(CO)_5^+$ representing the dominant product at all reaction times. Please note that a formal adsorption-stoichiometry $Pd_4O(CO)_y^+$ does not exclude the presence of $Pd_4(CO_2)(CO)_{y-1}^+$ complexes. The kinetic data reveal that Pd_4CO^+ is formed first, but the signal disappears after about 0.4 s. The adsorption of CO as the first reaction step is in agreement with the fact that the rate constants determined for the adsorption of CO onto Pd_4^+ is more than two orders of magnitude larger than the O_2 adsorption rate constant (cf. Figure 1a and Table 1). Also, the single product $Pd_4O_4^+$, which is detected when only O_2 is the reaction gas (see discussion above), is not observed at all in the presence of a O_2/CO reaction gas mixture.

Furthermore, a comparably large O_2 desorption rate constant was found for $Pd_4O_2^+$ (cf. Figure 1b), although it can be assumed that CO does not desorb from Pd_4^+ because CO binds strongly (experimental value determined from the measured rate constant: 132 ± 7 kJ mol^{-1}, theoretical value: 132.2 kJ mol^{-1}[40h]), resulting in an extremely small rate constant for decomposition of Pd_4CO^+ (cf. Figure 1b). Thus, the adsorption of CO can be considered the first adsorption step even under O_2-rich pressure conditions, and the adsorption of multiple CO is also likely, as was observed in the experiment.

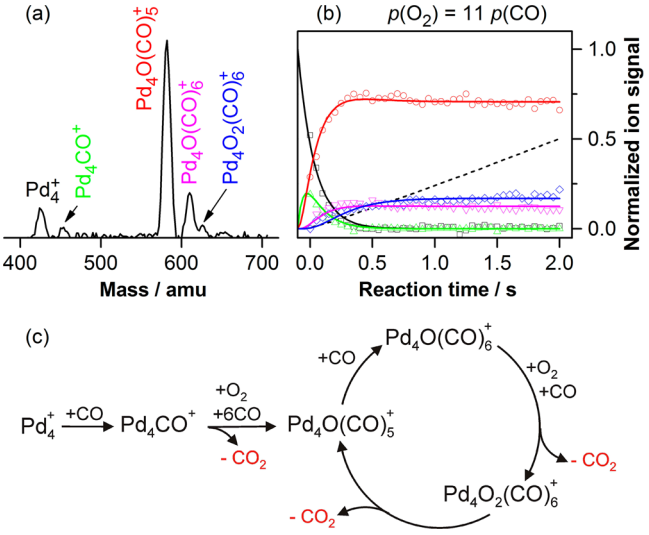

Figure 2. (a) Ion mass distribution (0.1 s reaction time) and (b) kinetics (open symbols) obtained from the reaction between Pd_4^+ and a 11:1 O_2/CO mixture at room temperature ($p(O_2)$ = 0.100 Pa, p(CO) = 0.009 Pa). The dashed line indicates the CO_2 production simulated on the basis of the proposed mechanism. (c) Proposed reaction mechanism that best fits the experimental data under these pressure conditions. The solid lines in (b) are obtained by fitting the integrated rate equations of this mechanism to the experimental data.

Additional reactivity experiments with already preoxidized Pd_4O^+ and an oxygen-rich O_2/CO mixture result in identical ion mass distributions, as observed for the bare Pd_4^+ (Figure 2a). The room-temperature reaction of Pd_4O^+ with O_2 only has recently been shown[36] to result in the formation of $Pd_4O_3^+$ and $Pd_4O_5^+$, whereas Pd_4O^+ reacts with CO to yield Pd_4^+ through formation and desorption of CO_2.[39] Consequently, the observation of identical product ion mass distributions for both Pd_4O^+ and Pd_4^+ lacking any of the typical oxidation products $Pd_4O_3^+$, $Pd_4O_4^+$, or $Pd_4O_5^+$ leads to the conclusion that CO adsorption must represent the first and dominating reaction step. In the case of Pd_4O^+, this first yields the bare palladium tetramer, which then further reacts to form the typical Pd_4^+ reaction products.

With respect to the measured reaction kinetics (Figure 2b), it is important to note that all observed products (except Pd_4CO^+) exhibit constant, nonvanishing concentrations after about 0.5 s reaction time. This is indicative of an equilibrium reaction mechanism. As the products $Pd_4O(CO)_5^+$ and $Pd_4O(CO)_6^+$ do contain dissociated oxygen, CO_2 must have been liberated in the process of formation of these products. Any conceivable alternative (liberation of C + O + O, O + CO, or O_2 + C) is clearly thermodynamically unfavorable compared to the liberation of CO_2. In most cases, the energy required to liberate a bound O or C atom will exceed other binding energies in the cluster complex, and thus, the cluster will decompose, which is not observed for the cluster systems investigated here. Hence, it is clear that CO_2 is liberated during the formation of the respective products, even though only charged species are measured directly in the present experimental setup. However, to sustain equilibrium reactions between these products and $Pd_4O_2(CO)_6^+$, CO_2 would be required to be present in the ion trap, which is not the case. The concentration of the catalytically formed CO_2 is about 6 orders of magnitude smaller than the concentrations of O_2 and CO and can thus be neglected.[42] This is clearly an excess

DOI: 10.1021/cs5016222
ACS Catal. 2015, 5, 2275−2289

reactant situation according to the principle of Le Chatelier, even considering the involvement of palladium as a catalyst. As a consequence, the forward CO_2 formation reaction is strongly favored—expressed differently: forward CO_2 formation must occur exclusively as the CO and O_2 concentrations are constant in the experiment, and CO_2 will leave the ion trap. Thus, the measured equilibrium type reaction kinetics cannot be explained by a simple equilibrium mechanism. Consequently, the only conceivable explanation for the constant, nonvanishing product concentrations in the kinetics is a catalytic reaction cycle.

A possible reaction mechanism including such a catalytic reaction cycle, which is proposed on the basis of the observed ion mass distributions and kinetics and which best fits the kinetic data, is displayed in Figure 2c. This mechanism shows that CO oxidation is indeed possible in the case of Pd_4^+, yet, interestingly, with the (pre-) oxidized (and apparently CO covered) cluster as catalytically active species. We note that here, and elsewhere in this paper, we refer to Pd_xO^+ (x = 4–6) as the (mono) oxidized cluster, or (pre-) oxidized cluster, to distinguish it from the bare Pd_x^+ cluster serving as a catalyzing substrate for the CO oxidation reaction. Similarly, we refer to $Pd_xO_y^+$ clusters as oxide (or nano-oxide) clusters. This, by itself, does not imply that these oxygen-containing clusters have the same stoichiometry, structure, or properties as the bulk oxide (PdO) or the surface oxides reviewed in the introductory section; we remark here that even in the case of extended surface systems, the electronic properties of the ultrathin surface oxides (see discussion in section 1.A), for example, Pd_5O_4 formed[9b] on Pd(111), differ greatly from those of the bulk oxide; in particular, the former catalyzes the CO oxidation reaction, whereas the latter (PdO) does not. To distinguish between chemisorbed oxygen atoms and "oxidic" oxygens would require high-resolution core spectroscopy measurements (see, e.g., ref 9b) that are outside the scope of our gas phase ion-trap measurements.

As stated above, recent reactivity studies of preoxidized Pd_4O^+ (and also $Pd_4O_2^+$) containing atomic oxygen with CO showed the fast formation and desorption of CO_2 under reformation of the bare cluster Pd_4^+.[39] Thus, it can be assumed that carbon dioxide is formed fast as soon as O_{ad} and CO_{ad} are coadsorbed on the cluster and in agreement with studies on Pd single crystals as well as supported nanoparticles and clusters, the reaction is largely determined by dissociative O_2 adsorption and the adsorption strength of CO.[3b,21b] We note here that no additional oxygen was supplied to the ion trap in these previous experiments,[35] and hence, no coadsorption products were observed in these cases for Pd_4^+, in contrast to the present experiments, in which a large oxygen excess was employed.

Separate adsorption experiments performed with only CO_2 in the ion trap demonstrate that all the clusters interact very weakly with carbon dioxide (very similar to the results of surface studies and in accordance with our calculations for Pd_6^+ shown below). At room temperature only the clusters with three and four palladium atoms exhibit noticeable CO_2 adsorption signals and only at comparably high partial pressures of >10% CO_2 in the ion trap. This confirms the facile desorption of readily formed CO_2. In addition, CO_2 is found to be easily replaced by coadsorbed carbon monoxide molecules.[39]

Due to the slow O_2 adsorption and dissociation in conjunction with the strong CO binding at room temperature, the CO combustion reaction on Pd_4^+ is, however, apparently not very effective, and the cluster is covered by five to six CO molecules, even under O_2-rich pressure conditions. This conclusion is supported by the comparably small catalytic turnover frequency of 0.26 ± 0.05 CO_2 molecules per second and cluster (which has been determined for Pd_4^+ from the kinetics in Figure 2b by simulating the emerging CO_2 product concentration as a function of the reaction time on the basis of the deduced rate constants) compared to, for example, 2.3 ± 0.5 CO_2 molecules per second for Pd_6O^+ (see also discussion below).

On Pd(111), the CO oxidation becomes effective, if the temperature exceeds about 450 K.[3b] The desorption of CO is the key for opening surface sites to activate O_2. At this temperature, the rate constant for CO desorption[6c] has been determined to amount to between 0.15 s^{-1} and 5 × 10^{-4} s^{-1}. This value is several orders of magnitude larger than the estimated room-temperature decomposition rate constant for Pd_4CO^+ (k_e = 1.1 × 10^{-21} cm^3 s^{-1} and k_{-1} ∼ 10^{-7} s^{-1}, respectively (cf. eq 6, p(He) = 1 Pa)). Considering the binding energy of CO to Pd_4^+ (132 ± 7 kJ mol^{-1}) determined in the present study, a rough estimate reveals that also for Pd_4^+ a reaction temperature of at least 380 K would be required to achieve desorption rate constants of >5 × 10^{-4} s^{-1}, which is in surprisingly good agreement with the effective CO oxidation conditions on Pd single crystals. Nevertheless, in the present cases, the mass spectra in Figure 2a indicate that chemisorbed O and CO coexist on a particle even at room temperature, which hints toward fundamental differences between the catalytic mechanisms and supports the suggestion that the (pre-) oxidized palladium clusters are the actual active catalysts.

3.C. CO Oxidation Mediated by Pd_5^+. In the case of the cluster Pd_5^+, both the O_2 and CO adsorption rates increase compared to the case of the Pd_4^+ cluster, cf. Figure 1a and Table 1. However, the O_2 desorption is less likely, whereas the CO desorption rate is found to increase for Pd_5^+, cf. Figure 1b and Table 1. This has profound consequences for the catalytic activity of this cluster Pd_5^+.

Figure 3a displays a representative ion mass distribution detected after the reaction of Pd_5^+ with a 13:1 O_2/CO mixture for 0.1 s, showing the oxygen-rich products $Pd_5O_3^+$, $Pd_5O_4^+$, $Pd_5O_3CO^+$, as well as the CO-rich $Pd_5O(CO)_6^+$. The preferred occurrence of oxygen-rich products at early reaction times reflects the increased O_2 adsorption and decreased O_2

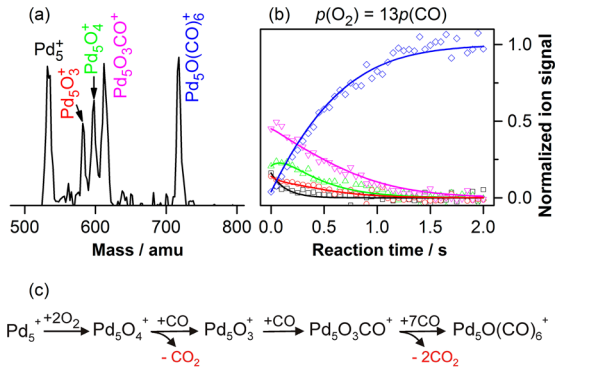

Figure 3. (a) Ion mass distributions (0.1 s reaction time) and (b) kinetics (open symbols) obtained from the reaction between Pd_5^+ and a 13:1 O_2/CO mixture at room temperature ($p(O_2)$ = 0.100 Pa, p(CO) = 0.008 Pa). (c) Proposed reaction mechanism that best fits the experimental data under these pressure conditions. The solid lines in (b) are obtained by fitting the integrated rate equations of this mechanism to the experimental data.

DOI: 10.1021/cs5016222
ACS Catal. 2015, 5, 2275–2289

desorption rate constant compared to Pd_4^+ (cf. Figure 1). Because oxidation studies of Pd_5^+ revealed $Pd_5O_4^+$ as the only reaction product,[35b,36] the formation of $Pd_5O_3^+$ and $Pd_5O_3CO^+$ in the presence of an O_2/CO mixture gives first indications for a successful CO oxidation mechanism at these early reaction times (t_R < 1.0 s).

At longer reaction time, however, the complexes $Pd_5O_3^+$, $Pd_5O_4^+$, $Pd_5O_3CO^+$ completely disappear, and the CO-rich product, $Pd_5O(CO)_6^+$, remains the only observable reaction product (see kinetics in Figure 3b). This observation indicates that the reaction of adsorbed O with CO is fast and facile also in the case of Pd_5^+, but only as long as not too many CO are adsorbed. The cluster-size-dependent competition between CO adsorption and combustion on oxidized palladium clusters has been detailed in a previous contribution.[39] The dominant CO adsorption is in line with the enhanced CO adsorption rate constant of this cluster, as apparent from Figure 1a. In the process of the formation of the final product, $Pd_5O(CO)_6^+$, CO_2 must again be formed and liberated. Yet, apparently no catalytic cycle is operative. The corresponding most simple reaction mechanism that best fits the kinetic data is depicted in Figure 3c.

3.D. CO Oxidation Mediated by Pd_6^+. *Room-Temperature CO Oxidation.* Pd_6^+ reacts with oxygen the strongest among the investigated clusters, exhibiting the largest O_2 adsorption rate constant and the smallest O_2 desorption rate constant (see Figure 1 and Table 1). The adsorption of O_2 can also compete strongly with the CO adsorption under the applied oxygen-rich conditions because both adsorption rate constants differ only by about 1 order of magnitude for Pd_6^+. But even more importantly, the CO desorption rate constant exceeds that of O_2 by about 3 orders of magnitude in the case of Pd_6^+ (cf. Figure 1b and Table 1). These facts are in line with the observation of mostly (essentially exclusively) oxygen-containing products, when Pd_6^+ is reacted with a 9:1 mixture of O_2 and CO for 0.1 s in the ion trap (see mass spectrum in Figure 4a).[35a] Apart from the main product, $Pd_6O_4^+$, additional ion signals corresponding to $Pd_6O_3^+$, $Pd_6O_5^+$, and $Pd_6O_5(CO)^+$ are detected. The odd number of oxygen atoms in these products and their immediate formation (cf. kinetics in Figure 4b) already leads us to expect Pd_6^+ to be the most active candidate for the catalytic oxidation of CO.

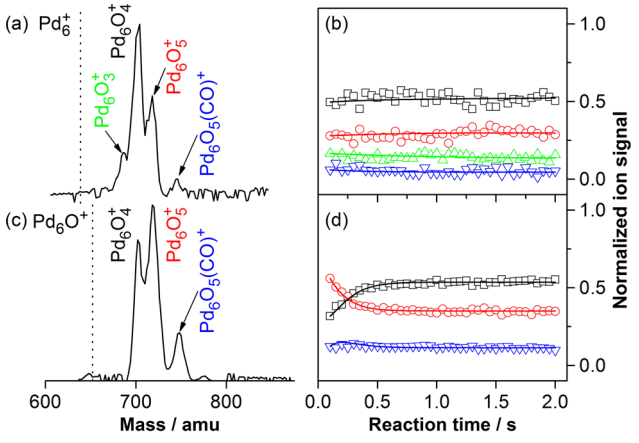

Figure 4. Representative ion mass distributions obtained at a reaction time of 0.1 s and corresponding kinetics of the reaction between (a,b) Pd_6^+ and O_2/CO as well as (c,d) Pd_6O^+ and O_2/CO recorded at 300 K. (a,b): $p(O_2)$ = 9 $p(CO)$ ($p(O_2)$ = 0.09 Pa, $p(CO)$ = 0.01 Pa); (c,d): $p(O_2)$ = 8 p(CO) ($p(O_2)$ = 0.040 Pa, $p(CO)$ = 0.005 Pa).

Indeed, $Pd_6O_4^+$ was detected as the sole product of the reaction of Pd_6^+ with O_2 over a large temperature range.[35a,36] The additional products, containing an odd number of oxygen atoms in the mass spectrum in Figure 4a, are only observed in the presence of an O_2/CO mixture, indicating the fast reaction of CO with the adsorbed oxygen leading to the release of CO_2. Analogous to Pd_4^+ (dashed black line in Figure 2b; TOF: 0.26 ± 0.05 CO_2 s^{-1}) also in the case of Pd_6^+ the rate of CO_2 release can be calculated yielding an about 1 order of magnitude larger value of 2.3 ± 0.5 s^{-1}.

The corresponding kinetic data (Figure 4b) show, under the applied experimental conditions, a rapid saturation of all products (faster than the time resolution of the experiment). Such kinetic data can either be explained by an equilibrium reaction mechanism with all products being connected by forward and backward reaction steps or by a reaction cycle. However, due to the elimination of oxygen atoms yielding $Pd_6O_3^+$, $Pd_6O_5^+$, and $Pd_6O_5(CO)^+$ which is only observed in the presence of CO, and the fact that atomic oxygen (or potentially liberated CO_2) is not present in the ion trap, an equilibrium reaction mechanism can be excluded. Thus, these products must be formed as part of a catalytic reaction cycle.

To gain more insight into the reaction mechanism the experiments have been repeated by exposing already preoxidized Pd_6O^+ to an oxygen-rich O_2/CO mixture. The result presented in Figure 4c shows a similar ion mass distribution as in the case of Pd_6^+ showing the products $Pd_6O_4^+$, $Pd_6O_5^+$, and $Pd_6O_5(CO)^+$, although $Pd_6O_3^+$ has not been detected under these particular experimental conditions. The corresponding kinetic data in Figure 4d reveal the fast formation of $Pd_6O_5^+$, which is in agreement with oxidation studies that yield $Pd_6O_5^+$ as the saturation product of the reaction between Pd_6O^+ and O_2 over a wide temperature range.[36] The intensity of the $Pd_6O_5^+$-signal then decreases and levels off at reaction times longer than 0.5 s. In contrast, the intensity of $Pd_6O_4^+$ increases at t_R < 0.5 s, identifying $Pd_6O_5^+$ as a precursor of $Pd_6O_4^+$.

The simplest reaction mechanism that fits best the experimental data of Pd_6^+ and Pd_6O^+, and which accounts also for the results of the oxidation experiments, is shown in Figure 5. The fits of the integrated rate equations of this

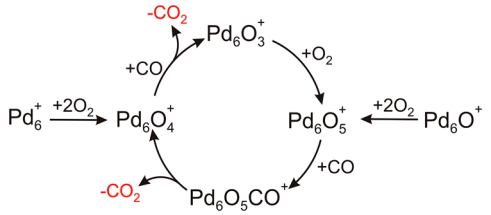

Figure 5. Proposed reaction mechanism that best fits the experimental data of Pd_6^+ and Pd_6O^+ shown in Figure 4b,d.

mechanism to the experimental data are displayed in Figure 4b,d as solid lines. In the following, the details of this catalytic reaction cycle will be discussed.

The dominance of the oxidation product $Pd_6O_4^+$ in the reaction of Pd_6^+ with O_2 and CO as well as the lack of products comprising only CO indicate the fast adsorption of two oxygen molecules as the first reaction steps. Because $Pd_6O_4^+$ was found to be oxidation resistant at room temperature,[35a] the product $Pd_6O_5^+$ cannot directly result from $Pd_6O_4^+$, but instead, $Pd_6O_3^+$

DOI: 10.1021/cs5016222
ACS Catal. 2015, 5, 2275−2289

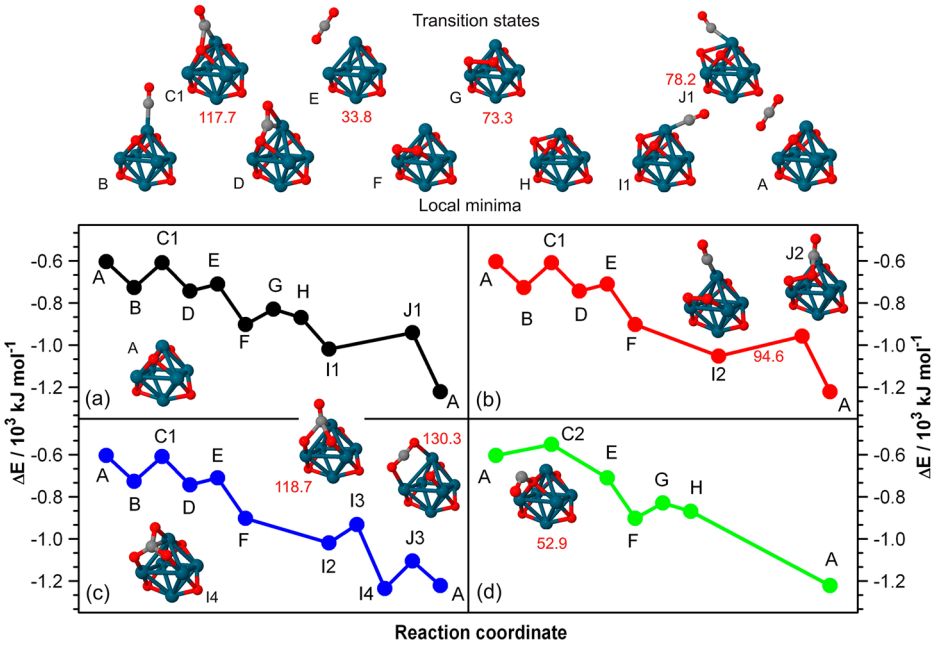

Figure 6. Calculated reaction pathways for the $Pd_6O_4^+$-catalyzed oxidation of CO.[35a] Three different Langmuir–Hinshelwood mechanisms (with both reactants adsorbed on the catalyst) are given by (a) black, (b) red, and (c) blue symbols while an alternative Eley–Rideal mechanism (one reactant adsorbed and the other impinging from the gas phase, green symbols) is displayed in (d). Atomic configurations corresponding to the transition states and the local potential energy minima are shown above the graphs in the first and second row, respectively. The TS barrier energies are given in red next to the TS configurations (the desorption energy for the first CO_2 molecule in black) in kJ mol^{-1}. Pd, O and C atoms are represented by blue, red and gray spheres, respectively.

must be formed through the reaction with a first CO molecule and the formation and desorption of CO_2 in the subsequent reaction step. $Pd_6O_3^+$ can then adsorb an additional O_2 molecule yielding $Pd_6O_5^+$. Due to the rather small intensity of the product $Pd_6O_3^+$ in the mass spectrum, it can be assumed that this reaction step proceeds at a fast rate. The next reaction step must then describe the interaction with a second CO molecule yielding $Pd_6O_5CO^+$, which represents a precursor for the desorption of a second CO_2 molecule that leads to the reformation of $Pd_6O_4^+$.

An identical catalytic reaction cycle can also be found for Pd_6O^+ with the exception of the entrance channel. In both cases, that is, starting from Pd_6^+ or from Pd_6O^+, the first reaction steps are represented by the adsorption of two oxygen molecules yielding $Pd_6O_4^+$ and $Pd_6O_5^+$, respectively. The formation of different products in the entrance channel is evident from the kinetic data showing increased ion intensity of $Pd_6O_5^+$ for the reaction of Pd_6O^+ that decreases at longer reaction times, whereas for Pd_6^+, the product $Pd_6O_4^+$ represents the main product in the whole investigated reaction time range.

Furthermore, from the reaction cycle (Figure 5), determined on the basis of the experimental data, it becomes clear that Pd_6^+ itself is not part of the catalytic cycle but that instead the nano-oxide cluster $Pd_6O_4^+$ is identified as the catalytically active reaction center. This experimental observation strongly supports the theoretical predictions that CO_2 formation is most effective under reaction conditions where preformation of supported nano-oxide clusters Pd_xO_y/MgO is possible.[21c,d,26] In contrast, in previous CO oxidation experiments with platinum and gold clusters, the bare metal clusters $Pt_x^{\pm}$ and Au_x^-, respectively, were found to be part of the catalytic cycle instead of the corresponding oxides.[53] Furthermore, the studies on Pd_6^+ show that dissociatively adsorbed oxygen O(ad) represents an active species for CO oxidation, as has been found also on Pd(111) and Pd(100) surfaces.[8b,54] However, recent reactivity studies[39] revealed that CO_2 formation is not efficient enough on the mono-oxide Pd_6O^+, so that apparently the highly oxidized clusters, such as $Pd_6O_4^+$ or $Pd_6O_5^+$, represent the more active catalytic species.

In comparison with Pd_4^+ and Pd_5^+, the Pd_6^+ cluster is considerably more active in promoting the conversion of CO to CO_2 under O_2-rich pressure conditions. From the kinetics in Figure 4d, a catalytic turnover frequency (TOF) of 2.3 ± 0.5 CO_2 molecules per second and per Pd_6^+ cluster can be determined, which is about one order of magnitude larger than the per-cluster TOF deduced for Pd_4^+ above (0.26 ± 0.05 CO_2 s^{-1}). It is also interesting to compare these values (measured at 300 K) to TOFs obtained by employing single crystal surfaces. For a Pd(111) surface, for example, a TOF of about 0.6 CO_2 s^{-1} per surface Pd atom site has been determined at 470 K and $p(CO)$ = 133 Pa, $p(O_2)$ = 67 Pa.[4] In these experiments, the TOF was found to decrease linearly with the oxygen pressure and to depend on the temperature in an Arrhenius-type relation in the investigated temperature range (470 to 570 K).

The major reasons for the apparently superior performance of the Pd_6^+ nanocatalyst can be found in the high reactivity toward O_2, which leads to the facile formation of stable $Pd_6O_y^+$ complexes,[35a,36] in combination with a rather small CO binding energy to Pd_6^+ (103.3 kJ mol^{-1}[40h]) that leads to a rate constant for CO desorption (k_{-1} = 1.1 s^{-1}) at room temperature, which is several orders of magnitude larger than for Pd_4^+ (k_{-1} = 2.6 × 10^{-7} s^{-1}), Pd_5^+ (k_{-1} = 6.5 × 10^{-5} s^{-1}), and also for extended palladium surfaces (k_{-1} = 10^{-9} – 10^{-12} s^{-1}[16b,c]).

Reaction Energetics. To gain more detailed insight into the energetics of the catalytic CO combustion reaction mediated by $Pd_6O_4^+$ and to allow for a quantitative comparison with the previous studies on extended Pd surfaces and on supported Pd nanoparticles, first-principles DFT calculations have been

DOI: 10.1021/cs5016222
ACS Catal. 2015, 5, 2275–2289

performed. Figure 6 displays four different possible reaction pathways along with the atomic configurations that correspond to the transition state barriers and local potential energy minima.

The first reaction mechanism (Figure 6a) follows a Langmuir–Hinshelwood scheme where the reaction occurs through interaction of adsorbed molecules and atoms. The sequence of steps starts with the barrier-free adsorption of a first CO molecule on the tetroxide cluster $Pd_6O_4^+$ (configuration A) yielding $Pd_6O_4CO^+$ (configuration B, CO binding energy $E(CO)$ = 122.6 kJ mol^{-1}). The adsorbed CO molecule reacts with an oxygen atom of $Pd_6O_4^+$ (activation barrier E_b = 117.7 kJ mol^{-1}, configuration C1) which results in the complex D. CO_2 is formed in this reaction step on the cluster in a bent configuration with an O–C–O angle of about 113° in the transition state C1. Subsequent reaction steps then involve the desorption of the formed CO_2 molecule yielding $Pd_6O_3^+$ (configuration E, $E(CO_2)$ = 33.8 kJ mol^{-1}), and the adsorption of an oxygen molecule resulting in $Pd_6O_5^+$ (configuration F, $E(O_2)$ = 192.1 kJ mol^{-1}, d(O–O) = 1.38 Å). This activated O_2 molecule (d(O–O) is larger by 0.13 Å compared to the bond length in the gaseous O_2 molecule) dissociates in an activated process (E_b = 73.3 kJ mol^{-1}, configurations F → G → H, d(O–O) = 2.8 Å in H) before the barrier-free adsorption of a second CO molecule ($E(CO)$ = 150.6 kJ mol^{-1}), yielding the experimentally observed complex $Pd_6O_5CO^+$ (configuration I1). CO_2 is formed on the cluster via the transition state J1. Here the adsorbed CO_2 has a bent geometry comparable to the preceding reaction step (O–C–O angle: 126°). The catalytic cycle is closed by reformation of $Pd_6O_4^+$ (configuration A) and CO_2 liberation involving an activation barrier of E_b = 78.2 kJ mol^{-1} (configurations I1 → J1 → A). The energy released in this last reaction step amounts to 203 kJ mol^{-1} and will initially lead to a vibrational excitation of the $Pd_6O_4^+$ cluster and also to an excitation of the desorbing CO_2 before thermalization in the buffer gas. Consistent with the experimentally proposed mechanism (Figure 5), the calculations also show that structure H can be formed also in the reaction of Pd_6O^+ with two O_2 molecules.

Two alternative pathways, also following a Langmuir–Hinshelwood reaction mechanism, are displayed in Figure 6b,c. In both cases, the first reaction steps starting from $Pd_6O_4^+$ (configuration A) and resulting in $Pd_6O_5^+$ (configuration F) are identical to the pathway in Figure 6a. However, in the pathway presented in Figure 6b, the molecularly adsorbed O_2 does not dissociate on the cluster, but instead, CO is directly adsorbed on configuration F ($E(CO)$ = 150.6 kJ mol^{-1}) leading to barrier-free formation of I2. Subsequent reaction of CO with an oxygen atom and desorption of CO_2 involves an activation barrier of E_b = 94.6 kJ mol^{-1} (configurations I2 → J2 → A). The pathway in Figure 6c is identical to the previous one until the formation of I2. Then it proceeds via the activated formation of an intermediate I4 (configurations I2 → I3 → I4, E_b = 118.7 kJ mol^{-1}) containing a partially negatively charged (δ = 0.7e) $CO_3^{-\delta}$ unit, as well as the activated formation and desorption of CO_2 (configurations I4 → J3 → A, E_b = 130.3 kJ mol^{-1}). Interestingly, in the transition state J3 just before desorption, the CO_2 molecule exhibits an almost linear geometry in contrast to the transition states discussed above.

Finally, Figure 6d displays an alternative reaction pathway following an Eley–Rideal mechanism where the reaction occurs between an impinging gas phase molecule and an adsorbed species. According to this Eley–Rideal reaction mechanism, the CO molecule directly adsorbs on an oxygen atom of $Pd_6O_4^+$ (configuration A) and leads to the formation (in a strongly bent transition state geometry) and desorption of a first CO_2 molecule, which involves a small activation barrier of E_b = 52.9 kJ mol^{-1} (configuration C2) and results in $Pd_6O_3^+$ (configuration E). This oxide adsorbs another O_2 molecule (configuration F) and undergoes activated structural rearrangement (configuration G, E_b = 73.3 kJ mol^{-1}), yielding configuration H, as already observed in the Langmuir–Hinshelwood pathway in Figure 6a. The subsequent adsorption of a second CO molecule and the formation and liberation of CO_2 is barrier-free.

Thus, these predicted reaction pathways demonstrate that the occurrence of effective room-temperature oxidation of CO with molecular oxygen promoted by $Pd_6O_4^+$ is possible, and they are completely consistent with the reaction mechanism determined on the basis of the experimental reaction kinetics data for Pd_6^+ and Pd_6O^+ (cf. Figure 5 and the discussion in section *Room-Temperature CO Oxidation*).

Comparison with Pd Surfaces. Figure 7a displays a schematic potential diagram illustrating the energetics of the CO oxidation reaction on a Pd(111) surface at low O_2 and CO coverages (corresponding to a temperature range of 500–700 K), which has been constructed by Ertl and co-workers on the basis of quantitative experimental data.[3b,55] Chemisorption of CO + 1/2 O_2 results in the liberation of an energy of about 257 kJ mol^{-1} (E_b(CO) = 142 ± 4 kJ mol^{-1}[16b,55] and E_b(O) = 115 kJ mol^{-1}; note that oxygen will experience recombinative molecular desorption at higher temperatures than CO),[56] which is dissipated in the solid. The formation of a carbon

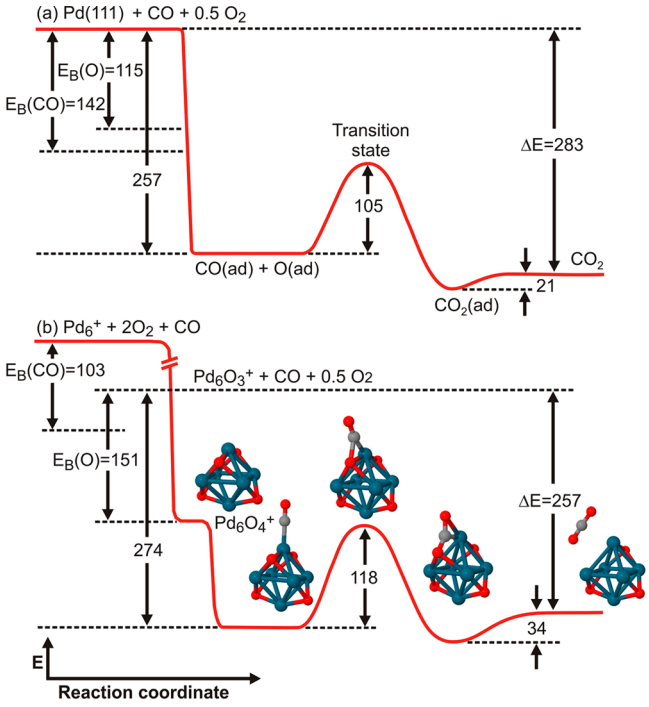

Figure 7. Schematic potential diagrams (energies in kJ mol^{-1}) for the CO oxidation on (a) a Pd(111) single crystal at low coverages[3b,55] and (b) the $Pd_6O_4^+$ cluster. The diagram for Pd(111) has been constructed from quantitative experimental data, and the energies in the diagram for the palladium cluster have been obtained by theoretical simulations and correspond to the reaction steps which are associated with the structures A–E in Figure 6a–c.

DOI: 10.1021/cs5016222
ACS Catal. 2015, 5, 2275–2289

dioxide molecule on the surface, CO_2(ad), from the adsorbed CO(ad) and O(ad) represents an activated Langmuir–Hinshelwood process involving a barrier of 105 ± 8 kJ mol^{-1}, whereas the final liberation of CO_2 is only slightly activated by 21 kJ mol^{-1}.[3b,55]

The overall reaction CO + 1/2 O_2 → CO_2 is exothermic with a total energy gain of 283 kJ mol^{-1}.[3b,55] Nevertheless, a reaction temperature of at least about 450 K is required to enable CO_2 formation.[3b] The reasons for these high temperatures are, as discussed in section 1.1, not found in the height of the activation barriers but rather in the strong binding of CO to palladium, which leads to CO poisoning of the surface at lower temperatures (in particular at elevated CO pressures) and thus inhibits O_2 coadsorption and consequently a quenching of the reaction.

A comparable potential diagram for the CO combustion reaction mediated by the free nano-oxide $Pd_6O_4^+$ is shown in Figure 7b. The energies and atomic structures displayed in this figure are equivalent to the theoretically obtained transition states and local minima A to E of Figure 6. For a direct comparison with the energetics on a Pd(111) surface, the sum of the average binding energy of one oxygen atom in $Pd_6O_4^+$ (151 kJ mol^{-1}[35a]) and the binding energy of a first CO molecule to $Pd_6O_4^+$ (123 kJ mol^{-1}) are given, resulting in a total energy of 274 kJ mol^{-1} for the formation of configuration B. This energy gain is only slightly larger than the energy gained upon adsorption of CO and 1/2 O_2 onto a Pd(111) surface. Configuration B then transforms into configuration D in a process that entails an activation barrier of 118 kJ mol^{-1} (configuration C1). This barrier is equivalent to the Langmuir–Hinshelwood barrier shown in Figure 7a.

The calculated activation energy for the analogous reaction of an adsorbed CO molecule with one oxygen atom of $Pd_6O_5^+$ amounts to 78 kJ mol^{-1} (transition state J1 in Figure 6a) or 94.6 kJ mol^{-1} (transition state J2), respectively. Thus, the type of adsorbed oxygen atoms decisively influences the activation energy of CO_2 formation. This is very much in line with UHV surface studies (see, e.g., introductory review in ref 57): The "classical" Langmuir–Hinshelwood activation energy of this reaction determined by Ertl and co-workers[3b,55] amounts to 105 kJ mol^{-1} at low CO pressures and reduces to 59 kJ mol^{-1} at moderate CO pressures due to a rearrangement of the oxygen adlayer. Varying activation energies for the CO combustion reaction with varying oxygen adsorption geometry have also been observed by other authors.[58] Subsequent desorption of the formed CO_2 molecule involves a second activation barrier of 34 kJ mol^{-1}, which is also very close to the experimental value of 21 kJ mol^{-1} obtained on a Pd(111) surface.

From Figure 7, it is thus apparent that the overall energetics of the CO oxidation reaction catalyzed by a Pd(111) surface and that on the $Pd_6O_4^+$ cluster, respectively, exhibit some remarkable similarities while also displaying fundamental differences like, for example, the oxide cluster being the active catalyst in the present case. One further important difference between these two catalytic systems is the binding behavior of carbon monoxide, and this difference determines that, in the case of $Pd_6O_4^+$, the catalytic CO combustion is possible already at room temperature (and below, see next section), whereas for the Pd surface, at least a temperature of 450 K is required for the reaction to proceed.

The CO bond strength to a Pd(111) surface is largely independent (at low coverages) of whether oxygen is already present on the surface or not. In addition, the value of the CO binding energy (142 kJ mol^{-1}) clearly exceeds the binding energy of oxygen atoms, which amounts to 115 kJ mol^{-1}. In contrast, the CO binding energy to a bare Pd_6^+ cluster is only 103 kJ mol^{-1},[40h] hence, considerably less than the enhanced binding of the oxygen atoms in $Pd_6O_4^+$ of 151 kJ mol^{-1}. This low CO binding energy determines the desorption rate of CO from Pd_6^+ (as shown in Figure 1) and, thus, the temperature for effective CO_2 formation. Once the nano-oxide $Pd_6O_4^+$ is formed, the CO binding energy is increased to 123 kJ mol^{-1}, which, however, does not affect the facile CO_2 formation.

Although the Langmuir–Hinshelwood barrier for CO_2 formation is slightly higher and the overall energy gain of the reaction is smaller on the free $Pd_6O_4^+$ compared to a Pd(111) surface, the considerably reduced CO binding energy on the bare Pd_6^+ results in a large desorption rate, protecting the cluster from CO poisoning and facilitating O_2 coadsorption at considerably lower temperatures. For comparison, the CO desorption rate constant from Pd_6CO^+, at 300 K, is $k_{-1} \sim 1$ s^{-1} (= $k_e = 4.4 \times 10^{-15}$ cm^{3}s^{-1} assuming p(He) = 1 Pa, cf. Figure 1b). Due to the high CO binding energy of 142 kJ mol^{-1} on a Pd(111) single crystal,[6b] similar rate constants can only be achieved at about 515 K. At this temperature, CO oxidation has been observed to occur.[3b]

Temperature Dependence. In the above, it has been demonstrated that the oxidation of CO by molecular oxygen catalyzed by $Pd_6O_4^+$, takes place even at room temperature. In order to evaluate the range in which low temperature catalytic conversion is possible, temperature-dependent measurements have been performed by cooling the ion trap in steps of 20 K down to cryogenic temperatures. At each temperature, product ion mass spectra were recorded after the reaction of Pd_6O^+ with O_2 and CO for t_R = 0.1 s in the ion trap. The results of these experiments are shown in Figure 8 in a 2D contour plot representation.

Under the given experimental conditions, the products $Pd_6O_3^+$, $Pd_6O_4^+$, $Pd_6O_5^+$, and $Pd_6O_5CO^+$ are observed in the mass spectrum at room temperature. This ion mass distribution remains unchanged upon cooling the ion trap down to about

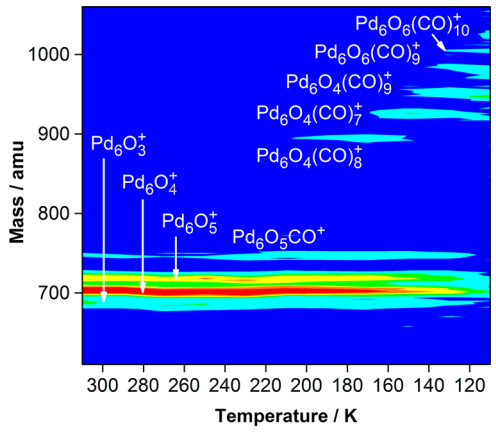

Figure 8. Two-dimensional contour plot representation of the temperature-dependent reaction of Pd_6O^+ with O_2 and CO (recorded in steps of 20 K, t_R = 0.1 s), illustrating the effective CO oxidation reaction over a wide temperature range between 300 K and about 190 K. $p(O_2)$ = 0.070 Pa, p(CO) = 0.006 Pa. Displayed are mass spectra as a function of temperature. The relative intensity of the mass signals is color coded ranging from blue (0%) to red (100%).

DOI: 10.1021/cs5016222
ACS Catal. 2015, 5, 2275–2289

190 K. However, below this temperature, the intensities of the room-temperature products decrease while new products appear. The recorded mass signals correspond to $Pd_6O_4(CO)_7^+$, $Pd_6O_4(CO)_8^+$, $Pd_6O_4(CO)_9^+$, $Pd_6O_6(CO)_9^+$, and $Pd_6O_6(CO)_{10}^+$. These products indicate that the CO adsorption is enhanced at very low temperatures and that apparently the CO oxidation is hindered accordingly at temperatures below 190 K.

These temperature-dependent ion mass distributions demonstrate that the catalytic CO oxidation is indeed possible at temperatures well below room temperature. However, the mass spectra also indicate the formation of CO-rich complexes $Pd_6O_y(CO)_z^+$ (y = 4, 6, z = 7−10) and thus the poisoning of the cluster by CO at temperatures below 190 K. This observation reflects a marked decrease of the rate constant for CO desorption (reduction of 6 orders of magnitude for 200 K compared to 300 K), which results in the formation of the complexes with multiple CO molecules.

Catalyst Poisoning versus Cooperative Effects. In section *Room-Temperature CO Oxidation*, it has been shown that an appropriate choice of the O_2/CO pressure ratio can compensate for differences in the termolecular CO and O_2 adsorption rate constants on Pd_6^+ (Table 1) and thus enable effective CO oxidation. However, the temperature-dependent experiments already indicated the possibility of CO poisoning of the Pd_6^+ cluster at temperatures below 190 K. For further insight into a potential catalyst poisoning, we studied next the reaction of Pd_6^+ with different O_2/CO mixtures at room temperature. Figure 9a,b display ion mass spectra and kinetic data obtained under O_2-rich conditions yielding the products $Pd_6O_3^+$, $Pd_6O_4^+$, $Pd_6O_5^+$, and $Pd_6O_5CO^+$, as already shown in Figure 4a,b and discussed in section *Room-Temperature CO Oxidation*. Decreasing the relative O_2 partial pressure ($p(O_2)$ = 0.7 p(CO), Figure 9c,d) leads to a decrease in the intensity of these products while additional new complexes $Pd_6O_2(CO)_6^+$, $Pd_6O_3(CO)_7^+$, as well as products comprising CO molecules only, $Pd_6(CO)_9^+$ and $Pd_6(CO)_{10}^+$, appear. The corresponding kinetics show fast formation of $Pd_6O_4^+$ and $Pd_6(CO)_9^+$, indicating a competition between O_2 and CO adsorption under these pressure conditions and thus a competition between CO combustion and CO poisoning. Furthermore, $Pd_6O_4^+$ and $Pd_6(CO)_9^+$ are precursors for the remaining products with $Pd_6O_2(CO)_6^+$ representing the stable final product. Most importantly, in contrast to the kinetic traces shown in Figure 9b, no equilibrium kinetics are observed anymore, which means that the potential catalytic CO_2 formation terminates because of the formation of the final product $Pd_6O_2(CO)_6^+$.

A further decrease in the O_2/CO pressure ratio ($p(O_2)$ = 0.1 p(CO), Figure 9e,f) leads to a complete shift in the ion mass distribution to the CO-rich products $Pd_6O_2(CO)_6^+$, $Pd_6O_3(CO)_7^+$, $Pd_6(CO)_9^+$, $Pd_6(CO)_{10}^+$, and $Pd_6(CO)_{11}^+$, whereas $Pd_6O_3^+$, $Pd_6O_4^+$, and $Pd_6O_5^+$ do not appear anymore in the mass spectrum. Under these CO-rich conditions, oxide formation is hampered, and the adsorption of CO is dominating the reaction. This results in the fast formation of $Pd_6(CO)_9^+$ (faster than the time-scale of the experiment), which represents the precursor for all other products. However, in contrast to extended Pd single-crystal surfaces, which are completely poisoned by CO under CO-rich conditions by site blocking for oxygen adsorption, the complex $Pd_6(CO)_9^+$ does not represent the final product. Instead, it serves as a precursor for the oxygen-containing complexes $Pd_6O_2(CO)_6^+$ and $Pd_6O_3(CO)_7^+$, as can be seen from the kinetic data in Figure 9f. This finding is in agreement with previous studies on small deposited Pd_x clusters for which preadsorbed CO was observed to promote oxygen adsorption and dissociation.[21b] Consequently, CO does not completely poison the small Pd_6^+ clusters; however, it can be concluded that CO oxidation is not effective anymore under CO-rich pressure conditions and the catalytic cycle terminates through formation of the final product $Pd_6O_2(CO)_6^+$.

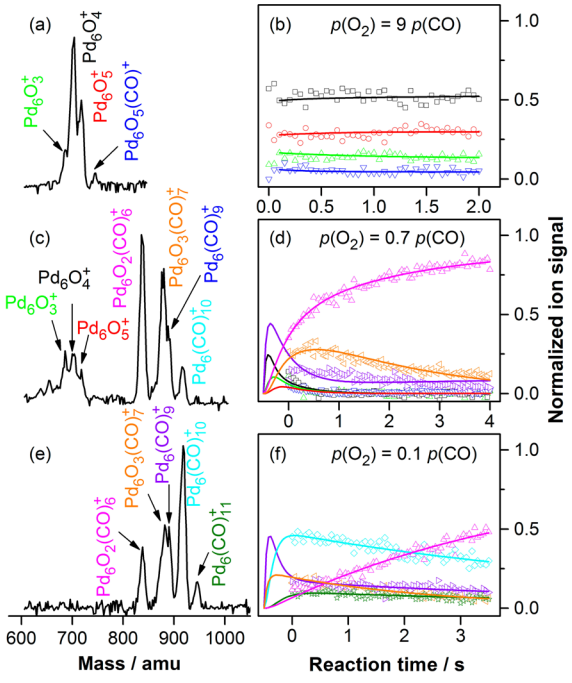

Figure 9. Pressure-dependent product ion mass distributions and corresponding kinetic data for the reaction of Pd_6^+ with O_2 and CO at room temperature showing the change from effective CO combustion under O_2-rich conditions to CO poisoning with increasing CO concentration. (a,b): $p(O_2)$ = 9 p(CO) ($p(O_2)$ = 0.09 Pa, p(CO) = 0.01 Pa), (c,d): $p(O_2)$ = 0.7 p(CO) ($p(O_2)$ = 0.010 Pa, p(CO) = 0.015 Pa); (e,f): $p(O_2)$ = 0.1 p(CO) ($p(O_2)$ = 0.01 Pa, p(CO) = 0.10 Pa).

4. CONCLUSION

In this paper, we reported on the comprehensive experimental and theoretical investigations of the catalytic low-temperature CO combustion reaction mediated by small free palladium clusters Pd_x^+ (x = 2−7) and their oxides Pd_xO^+ (x = 2−7). Utilizing ion trap mass spectrometry in conjunction with first-principles computations, we focused mainly on the clusters Pd_4^+, Pd_5^+, and Pd_6^+ and their oxides as model systems for studies of the kinetics and energetics of the catalytic CO oxidation reaction. The findings were interpreted on the basis of CO and O_2 adsorption and desorption rate constants and compared with previous investigations on Pd single-crystal surfaces as well as supported nanoparticles and small clusters.

For all investigated cluster sizes, the fast O_2 adsorption and dissociation and the CO binding strength were found to be the key factors that determine the effective CO oxidation. This is in agreement with previous studies on Pd single crystals and supported nanoparticles and clusters.

Strong CO binding to Pd_4^+ and Pd_5^+ inhibits effective low-temperature CO_2 formation even under oxygen-rich reaction conditions, whereas Pd_6^+ was identified as being particularly

DOI: 10.1021/cs5016222
ACS Catal. 2015, 5, 2275−2289

active in catalyzing this reaction in a temperature range between 300 and 190 K under O_2-rich pressure conditions. The superior catalytic properties of this particular cluster were attributed to the fast adsorption and dissociation of O_2 on Pd_6^+ yielding the nano-oxide $Pd_6O_4^+$ in conjunction with a comparably low CO bond strength to the palladium hexamer cluster. Furthermore, additional experiments utilizing the preoxidized cluster Pd_6O^+, as well as kinetic measurements, allowed an unambiguous determination of details of the catalytic reaction mechanism, revealing the nano-oxide $Pd_6O_4^+$ as the catalytically active species. At temperatures below 190 K and under excess of CO, the oxidation reaction of CO was observed to be impeded, and CO adsorption becomes the dominating process.

Complementary first-principles DFT computations of different possible reaction pathways allowed for molecular level insight into the energetics of the CO combustion reaction mediated by $Pd_6O_4^+$. These studies revealed surprising similarities but also fundamental differences between the reaction mechanism and the energetics of the CO oxidation reaction mediated by the free palladium clusters and the reaction on Pd(111) single crystals. A major difference was identified to arise from a considerably reduced CO bond strength on Pd_6^+ compared to Pd(111), which protects the Pd_6^+ cluster against CO poisoning at room temperature and below, thus enabling effective low-temperature cluster-catalyzed CO oxidation.

The findings of the present study, employing gas-phase clusters as model systems, are found to be generally consistent with previous studies on Pd single-crystal surfaces as well as on supported nanoparticles and clusters, and hence, they serve to demonstrate the complementarity between the gas-phase cluster science approach and surface science studies. Furthermore, our investigation shows that size effects in the O_2 and CO adsorption play an important role in this reaction in the case of small clusters. The observation of dramatic changes in the chemical and catalytic properties of small clusters by the mere addition or removal of one atom opens new possibilities for the rational design of effective low-temperature CO oxidation catalysts.

■ ASSOCIATED CONTENT

Supporting Information

The following file is available free of charge on the ACS Publications website at DOI: 10.1021/cs5016222.

Experimental details, description of techniques, and supplemental data (PDF)

■ AUTHOR INFORMATION

Corresponding Authors

*E-mail: thorsten.bernhardt@uni-ulm.de. Fax: (+49) 731-5025452.

*E-mail: uzi.landman@physics.gatech.edu. Fax: (+1) 404-894-7747.

Notes

The authors declare no competing financial interest.

■ ACKNOWLEDGMENTS

We gratefully acknowledge financial support by the Deutsche Forschungsgemeinschaft. In particular, S.M.L. is grateful to the European Social Fund Baden-Württemberg for a Margarete von Wrangell fellowship. The work of U.L. and R.N.B. at the Georgia Institute of Technology was supported by a grant from the U.S. AFOSR, with partial support to U.L. by the Office of Basic Energy Sciences of the U.S. Department of Energy under Contract No. FG05-86ER45234. Calculations were performed at the Georgia Institute of Technology Center for Computational Materials Science.

■ REFERENCES

(1) Gates, B. C. *Catalytic Chemistry*; John Wiley & Sons, Inc.: New York, Singapore, 1992.

(2) *Handbook of Heterogeneous Catalysis*; Ertl, G., Knözinger, E., Weitkamp, J., Eds.; Wiley-VCH: Weinheim, 1997; Vol. 4.

(3) (a) Conrad, H.; Ertl, G.; Küppers, J. *Surf. Sci.* **1978**, *76*, 323−342. (b) Engel, T.; Ertl, G. *J. Chem. Phys.* **1978**, *69*, 1267−1281.

(4) Szanyi, J.; Kuhn, W. K.; Goodman, D. W. *J. Phys. Chem.* **1994**, *98*, 2978−2981.

(5) (a) Nolan, P. D.; Lutz, B. R.; Tanaka, P. L.; Mullins, C. B. *Surf. Sci.* **1998**, *419*, L107−L113. (b) Guo, X.; Hoffman, A.; Yates, J. T., Jr. *J. Chem. Phys.* **1989**, *90*, 5787−5792.

(6) (a) Tracy, J. C.; Palmberg, P. W. *J. Chem. Phys.* **1969**, *51*, 4852−4862. (b) Ertl, G.; Koch, J. *Z. Naturforsch.* **1970**, *25 a*, 1906−1911. (c) Engel, T. *J. Chem. Phys.* **1978**, *69*, 373−385. (d) Bradshaw, A. M.; Hoffmann, F. M. *Surf. Sci.* **1978**, *72*, 513−535. (e) Behm, R. J.; Christmann, K.; Ertl, G.; Van Hove, M. A. *J. Chem. Phys.* **1980**, *73*, 2984−2995. (f) Duriez, C.; Henry, C. R.; Chapon, C. *Surf. Sci.* **1991**, *253*, 190−204. (g) Jones, I. Z.; Bennett, R. A.; Bowker, M. *Surf. Sci.* **1999**, *439*, 235−248. (h) Zorn, K.; Giorgio, S.; Halwax, E.; Henry, C. R.; Grönbeck, H.; Rupprechter, G. *J. Phys. Chem. C* **2011**, *115*, 1103−1111.

(7) Méndez, J.; Kim, S. H.; Cerdá, J.; Wintterlin, J.; Ertl, G. *Phys. Rev. B* **2005**, *71*, 085409.

(8) (a) Over, H.; Seitsonen, A. P. *Science* **2002**, *297*, 2003−2005. (b) Gabasch, H.; Knop-Gericke, A.; Schlögl, R.; Borasio, M.; Weilach, C.; Rupprechter, G.; Penner, S.; Jenewein, B.; Hayek, K.; Klötzer, B. *Phys. Chem. Chem. Phys.* **2007**, *9*, 533−540.

(9) (a) Carlisle, C. I.; King, D. A.; Bocquet, M.-L.; Cerdá, J.; Sautet, P. *Phys. Rev. Lett.* **2000**, *84*, 3899−3902. (b) Lundgren, E.; Kresse, G.; Klein, C.; Borg, M.; Andersen, J. N.; De Santis, M.; Gauthier, Y.; Konvicka, C.; Schmid, M.; Varga, P. *Phys. Rev. Lett.* **2002**, *88*, 246103. (c) Li, W.-X.; Stampfl, C.; Scheffler, M. *Phys. Rev. Lett.* **2003**, *90*, 256102. (d) Reuter, K.; Scheffler, M. *Appl. Phys. A: Mater. Sci. Process.* **2004**, *78*, 793−798.

(10) Schmid, M.; Leonardelli, G.; Sporn, M.; Platzgummer, E.; Hebenstreit, W.; Pinczolits, M.; Varga, P. *Phys. Rev. Lett.* **1999**, *82*, 355−358.

(11) Besenbacher, F.; Nørskov, J. K. *Prog. Surf. Sci.* **1993**, *44*, 5−66.

(12) (a) Surnev, S.; Kresse, G.; Ramsey, M. G.; Netzer, F. P. *Phys. Rev. Lett.* **2001**, *87*, 086102. (b) Dulub, O.; Hebenstreit, W.; Diebold, U. *Phys. Rev. Lett.* **2000**, *84*, 3646−3649.

(13) (a) Henry, C. R. *Surf. Sci. Rep.* **1998**, *31*, 231−325. (b) Goodman, D. W. *Surf. Rev. Lett.* **1995**, *2*, 9−24. (c) Nilius, N.; Risse, T.; Schauermann, S.; Shaikhutdinov, S.; Sterrer, M.; Freund, H.-J. *Top. Catal.* **2011**, *54*, 4−12.

(14) (a) Meusel, I.; Hoffmann, J.; Hartmann, J.; Heemeier, M.; Bäumer, M.; Libuda, J.; Freund, H.-J. *Catal. Lett.* **2001**, *71*, 5−13. (b) Penner, S.; Bera, P.; Pedersen, S.; Ngo, L. T.; Harris, J. J. W.; Campbell, C. T. *J. Phys. Chem. B* **2006**, *110*, 24577−24584. (c) Shaikhutdinov, S.; Heemeier, M.; Hoffmann, J.; Meusel, I.; Richter, B.; Bäumer, M.; Kuhlenbeck, H.; Libuda, J.; Freund, H.-J.; Oldman, R.; Jackson, S. D.; Konvicka, C.; Schmid, M.; Varga, P. *Surf. Sci.* **2002**, *501*, 270−281. (d) Schalow, T.; Laurin, M.; Brandt, B.; Schauermann, S.; Guimond, B.; Kuhlenbeck, H.; Starr, D. E.; Shaikhutdinov, S. K.; Libuda, J.; Freund, H.-J. *Angew. Chem., Int. Ed.* **2005**, *44*, 7601−7605.

(15) Henry, C. R.; Chapon, C.; Goyhenex, C. *Surf. Sci.* **1992**, *272*, 283−288.

(16) Stará, I.; Matolín, V. *Surf. Sci.* **1994**, *313*, 99−106.

DOI: 10.1021/cs5016222
ACS Catal. 2015, 5, 2275−2289

(17) Fischer-Wolfarth, J.-H.; Farmer, J. A.; Flores-Camacho, J. M.; Genest, A.; Yudanov, I. V.; Rösch, N.; Campbell, C. T.; Schauermann, S.; Freund, H.-J. *Phys. Rev. B* **2010**, *81*, 241416.
(18) Sitja, G.; Le Moal, S.; Marsault, M.; Hamm, G.; Leroy, F.; Henry, C. R. *Nano Lett.* **2013**, *13*, 1977−1982.
(19) Stará, I.; Nehasil, V.; Matolín, V. *Surf. Sci.* **1995**, *331*−*333*, 173−177.
(20) (a) Landman, U. *Solid State Commun.* **1998**, *107*, 693−708. (b) Landman, U.; Barnett, R. N.; Moseler, M.; Yannouleas, C. In *The Physics and Chemistry of Clusters, Proceedings of the Nobel Symposium 11*; Campbell, E. E. B., Larsson, M., Eds.; World Scientific: Singapore, 2001; pp 42−68. (c) Landman, U. *Proc. Nat. Acad. Sci. (USA)* **2005**, *102*, 6671−6678. (d) Sanchez, A.; Abbet, S.; Heiz, U.; Schneider, W.-D.; Häkkinen, H.; Barnett, R. N.; Landman, U. *J. Phys. Chem. A* **1999**, *103*, 9573−9578. (e) Landman, U.; Yoon, B.; Zhang, C.; Heiz, U.; Arenz, M. *Top. Catal.* **2007**, *44*, 145−158. (f) Bernhardt, T. M.; Heiz, U.; Landman, U. In *Nanocatalysis*; Heiz, U., Landman, U., Eds.; Springer-Verlag: Berlin, 2007; p 1−191;. (g) Lang, S. M.; Popolan, D. M.; Bernhardt, T. M. In *Atomic Clusters: From Gas Phase to Deposited*; Woodruff, P., Ed.; Elsevier: Amsterdam, 2007; Vol. *12*, pp 53−90.
(21) (a) Abbet, S.; Heiz, U.; Häkkinen, H.; Landman, U. *Phys. Rev. Lett.* **2001**, *86*, 5950−5953. (b) Kunz, S.; Schweinberger, F. F.; Habibpour, V.; Röttgen, M.; Harding, C.; Arenz, M.; Heiz, U. *J. Phys. Chem. C* **2010**, *114*, 1651−1654. (c) Moseler, M.; Walter, M.; Yoon, B.; Landman, U.; Habibpour, V.; Harding, C.; Kunz, S.; Heiz, U. *J. Am. Chem. Soc.* **2012**, *134*, 7690−7699. (d) Yoon, B.; Landman, U.; Habibpour, V.; Harding, C.; Kunz, S.; Heiz, U.; Moseler, M.; Walter, M. *J. Phys. Chem. C* **2012**, *116*, 9594−9607.
(22) Mars, P.; van Krevelen, D. W. *Chem. Eng. Sci.* **1954**, *3*, 41−59.
(23) (a) Kaden, W. E.; Wu, T.; Kunkel, W. A.; Anderson, S. L. *Science* **2009**, *326*, 826−829. (b) Kaden, W. E.; Kunkel, W. A.; Kane, M. D.; Roberts, F. S.; Anderson, S. L. *J. Am. Chem. Soc.* **2010**, *132*, 13097−13099.
(24) Wu, T.; Kaden, W. E.; Kunkel, W. A.; Anderson, S. L. *Surf. Sci.* **2009**, *603*, 2764−2770.
(25) Robles, R.; Khanna, S. N. *Phys. Rev. B* **2010**, *82*, 085428.
(26) Huber, B.; Koskinen, P.; Häkkinen, H.; Moseler, M. *Nat. Mater.* **2006**, *5*, 44−47.
(27) Reilly, N. M.; Johnson, G. E.; Castleman Jr., A. W. In *Model systems in catalysis: Single crystals to supported enzyme mimics*; Rioux, R. M., Ed.; Springer Science + Business Media: New York, 2010.
(28) Böhme, D. K.; Schwarz, H. *Angew. Chem., Int. Ed.* **2005**, *44*, 2336−2354.
(29) Lang, S. M.; Bernhardt, T. M. *Phys. Chem. Chem. Phys.* **2012**, *14*, 9255−9269.
(30) (a) Hintz, P. A.; Ervin, K. M. *J. Chem. Phys.* **1995**, *103*, 7897−7906. (b) von Gynz-Rekowski, F.; Ganteför, G.; Kim, D. Y. *Eur. Phys. J. D* **2007**, *43*, 81−84.
(31) (a) Bare, W. D.; Citra, A.; Chertihin, G. V.; Andrews, L. *J. Phys. Chem. A* **1999**, *103*, 5456−5462. (b) Huber, H.; Klotzbücher, W.; Ozin, G. A.; Voet, A. V. *Can. J. Chem.* **1973**, 2722−2736. (c) Andersson, M.; Rosén, A. *J. Phys.: Condens. Matter* **2010**, *22*, 334223.
(32) Ramond, T. M.; Davico, G. E.; Hellberg, F.; Svedberg, F.; Salén, P.; Söderqvist, P.; Lineberger, W. C. *J. Mol. Spectrosc.* **2002**, *216*, 1−14.
(33) (a) Huber, B.; Häkkinen, H.; Landman, U.; Moseler, M. *Comput. Mater. Sci.* **2006**, *35*, 371−374. (b) Roques, J.; Lacaze-Dufaure, C.; Mijoule, C. *J. Chem. Theory Comput.* **2007**, *3*, 878−884. (c) Wan, X.; Yoshizawa, K.; Ohashi, N.; Endou, A.; Takami, S.; Kubo, M.; Miyamoto, A.; Imamura, A. *Scripta mater.* **2001**, *44*, 1919−1923. (d) Kalita, B.; Deka, R. C. *J. Am. Chem. Soc.* **2009**, *131*, 13252−13254.
(34) Chen, Y.-M.; Armentrout, P. B. *J. Chem. Phys.* **1995**, *103*, 618−625.
(35) (a) Lang, S. M.; Fleischer, I.; Bernhardt, T. M.; Barnett, R. N.; Landman, U. *J. Am. Chem. Soc.* **2012**, *134*, 20654−20659. (b) Lang, S. M.; Frank, A.; Fleischer, I.; Bernhardt, T. M. *Eur. Phys. J. D* **2013**, *67*, 19.
(36) Lang, S. M.; Fleischer, I.; Bernhardt, T. M.; Barnett, R. N.; Landman, U. *J. Phys. Chem. A* **2014**, *118*, 8572−8582.
(37) (a) Spasov, V. A.; Ervin, K. M. *J. Chem. Phys.* **1998**, *109*, 5344−5350. (b) Hintz, P. A.; Ervin, K. M. *J. Chem. Phys.* **1994**, *100*, 5715−5725. (c) Gruene, P.; Fielicke, A.; Meijer, G.; Rayner, D. M. *Phys. Chem. Chem. Phys.* **2008**, *10*, 6144−6149.
(38) Cox, D. M.; Reichmann, K. C.; Trevor, D. J.; Kaldor, A. *J. Chem. Phys.* **1988**, *88*, 111−119.
(39) Lang, S. M.; Schnabel, T.; Bernhardt, T. M. *Phys. Chem. Chem. Phys.* **2012**, *14*, 9364−9370.
(40) (a) Blomberg, M. R. A.; Lebrilla, C. B.; Siegahn, P. E. M. *Chem. Phys. Lett.* **1988**, *150*, 522−528. (b) Goursot, A.; Papai, I.; Salahub, D. R. *J. Am. Chem. Soc.* **1992**, *114*, 7452−7458. (c) Schultz, N. E.; Gherman, B. F.; Cramer, C. J.; Truhlar, D. G. *J. Phys. Chem. B* **2006**, *110*, 24030−24046. (d) Pacchioni, G.; Chung, S.-C.; Krüger, S.; Rösch, N. *Surf. Sci.* **1997**, *392*, 173−184. (e) Pacchioni, G.; Koutecký, J. *J. Phys. Chem.* **1987**, *91*, 2658−2664. (f) Andzelm, J.; Salahub, D. *Int. J. Quantum Chem.* **1986**, *29*, 1091−1104. (g) Zanti, G.; Peeters, D. *Eur. J. Inorg. Chem.* **2009**, 3904−3911. (h) Kalita, B.; Deka, R. C. *Eur. Phys. J. D* **2009**, *53*, 51−58.
(41) Reber, A. C.; Khanna, S. N.; Tyo, E. C.; Harmon, C. L.; Castleman, A. W., Jr. *J. Chem. Phys.* **2011**, *135*, 234303.
(42) Bernhardt, T. M. *Int. J. Mass Spectrom.* **2005**, *243*, 1−29.
(43) Keller, R.; Nöhmeier, F.; Spädtke, P.; Schönenberg, M. H. *Vacuum* **1984**, *34*, 31−35.
(44) Schumacher, E. *DETMECH - Chemical Reaction Kinetics Software*; University of Bern: Chemistry Department, 2003.
(45) (a) Steinfeld, J. I.; Francisco, J. S.; Hase, W. L. *Chemical Kinetics and Dynamics*; 2nd ed.; Prentice Hall: Upper Saddle River, NJ, 1999. (b) Laidler, K. J. *Chemical Kinetics*, 3rd ed.; HarperCollins: New York, 1987.
(46) Bernhardt, T. M.; Hagen, J.; Lang, S. M.; Popolan, D. M.; Socaciu-Siebert, L.; Wöste, L. *J. Phys. Chem. A* **2009**, *113*, 2724−2733.
(47) Langevin, P. M. *Ann. Chim. Phys.* **1905**, *5*, 245−288.
(48) Barnett, R. N.; Landman, U. *Phys. Rev. B* **1993**, *48*, 2081−2097.
(49) Troullier, N.; Martins, J. L. *Phys. Rev. B* **1991**, *43*, 1993−2006.
(50) Perdew, J. P.; Burke, K.; Ernzerhof, M. *Phys. Rev. Lett.* **1996**, *77*, 3865−3868.
(51) (a) Moseler, M.; Häkkinen, H.; Barnett, R. N.; Landman, U. *Phys. Rev. Lett.* **2001**, *86*, 2545−2548. (b) Moseler, M.; Häkkinen, H.; Landman, U. *Phys. Rev. Lett.* **2002**, *89*, 176103.
(52) (a) Marcus, R. A. *J. Chem. Phys.* **1952**, *20*, 359−364. (b) Holbrook, K. A.; Pilling, M. J.; Robertson, S. H. *Unimolecular Reactions*, 2nd ed.; John Wiley & Sons Ltd.: Chichester, 1996.
(53) (a) Shi, Y.; Ervin, K. M. *J. Chem. Phys.* **1998**, *108*, 1757−1760. (b) Balaj, O. P.; Balteanu, I.; Roßteuscher, T. T. J.; Beyer, M. K.; Bondybey, V. E. *Angew. Chem., Int. Ed.* **2004**, *43*, 6519−6522. (c) Socaciu, L. D.; Hagen, J.; Bernhardt, T. M.; Wöste, L.; Heiz, U.; Häkkinen, H.; Landman, U. *J. Am. Chem. Soc.* **2003**, *125*, 10437−10445. (d) Wallace, W. T.; Whetten, R. L. *J. Am. Chem. Soc.* **2002**, *124*, 7499−7505.
(54) Zheng, G.; Altman, E. I. *J. Phys. Chem. B* **2002**, *106*, 1048−1057.
(55) Engel, T.; Ertl, G. In *The Chemical Physics of Solid Surfaces and Heterogeneous Catalysis*; King, D. A., Woodruff, D. P., Eds.; Elsevier: Amsterdam, 1982; Vol. *4*, pp 73−93.
(56) Conrad, H.; Ertl, G.; Küppers, J.; Latta, E. E. *Surf. Sci.* **1977**, *65*, 245−260.
(57) Farkas, A. P.; Diemant, T.; Bansmann, J.; Behm, R. J. *ChemPhysChem* **2012**, *13*, 3516−3525.
(58) (a) Matsushima, T.; Asada, H. *J. Chem. Phys.* **1986**, *85*, 1658−1668. (b) Kim, S. H.; Méndez, J.; Wintterlin, J.; Ertl, G. *Phys. Rev. B* **2005**, *72*, 155414.

DOI: 10.1021/cs5016222
ACS Catal. 2015, 5, 2275−2289